The Company of
Biologists

RESEARCH ARTICLE

Callose deposition is essential for the completion of cytokinesis in the unicellular alga *Penium margaritaceum*

Destiny J. Davis[1], Minmin Wang[1], Iben Sørensen[2], Jocelyn K. C. Rose[2], David S. Domozych[3] and Georgia Drakakaki[1],*

ABSTRACT

Cytokinesis in land plants involves the formation of a cell plate that develops into the new cell wall. Callose, a β-1,3 glucan, accumulates at later stages of cell plate development, presumably to stabilize this delicate membrane network during expansion. Cytokinetic callose is considered specific to multicellular plant species, because it has not been detected in unicellular algae. Here we present callose at the cytokinesis junction of the unicellular charophyte, *Penium margaritaceum*. Callose deposition at the division plane of *P. margaritaceum* showed distinct, spatiotemporal patterns likely representing distinct roles of this polymer in cytokinesis. Pharmacological inhibition of callose deposition by endosidin 7 resulted in cytokinesis defects, consistent with the essential role for this polymer in *P. margaritaceum* cell division. Cell wall deposition at the isthmus zone was also affected by the absence of callose, demonstrating the dynamic nature of new wall assembly in *P. margaritaceum*. The identification of candidate callose synthase genes provides molecular evidence for callose biosynthesis in *P. margaritaceum*. The evolutionary implications of cytokinetic callose in this unicellular zygnematopycean alga is discussed in the context of the conquest of land by plants.

This article has an associated First Person interview with the first author of the paper.

KEY WORDS: Callose, Cytokinesis, *Penium margaritaceum*, Cell plate

INTRODUCTION

Cytokinesis features have long been used in comparative biology to infer evolutionary relationships (Balasubramanian et al., 2004; Miyagishima et al., 2008; Stewart et al., 1973). Even though it has been extensively studied in all major kingdoms of life, the precise mechanism of cytokinesis and its change over evolutionary time remains one of cell biology's biggest mysteries (Hall et al., 2008; Pollard, 2017). In the green plant lineage, cytokinetic characteristics have largely been studied in the context of understanding the migration of green plants from aquatic to terrestrial habitats and the cell wall modifications that occurred during this transition (Buschmann and Zachgo, 2016; McBride, 1967).

The land plant cell wall provides the plant with several key adaptations to terrestrial life, including protection against abiotic stress and pathogen attack, structural support to the plant body and the integration of environmental and developmental signals (Hall et al., 2008; Popper and Tuohy, 2010; Sørensen et al., 2010). *De novo* formation of the land plant cell wall occurs during cytokinesis, as Golgi-derived vesicles carrying membrane and cell wall cargo coalesce at the plane of division to form a cell plate. The cell plate expands and matures centrifugally until it reaches the parental plasma membrane, thereby dividing the cytoplasm of the cell into two daughter cells (Drakakaki, 2015; Samuels et al., 1995; Seguí-Simarro et al., 2004; Smertenko et al., 2017). Callose, a β-1,3 glucan, is a vital luminal polysaccharide of the cell plate. This polymer is transiently incorporated into the cell plate, where it is thought to act as a stabilizing matrix for the delicate membrane network while also aiding in the radial expansion of the cell plate as it matures into a cell wall (Jawaid et al., 2020, preprint; Samuels et al., 1995). Both genetic studies and pharmacological inhibition of callose deposition during cytokinesis have shown the essential role of callose in *Arabidopsis thaliana* cell plate maturation (Chen et al., 2009; Park et al., 2014; Thiele et al., 2009). Specifically, without callose, cell plate maturation stalls, leading to its fragmentation and failed cytokinesis, resulting in binucleate cells (Chen et al., 2009; Guseman et al., 2010; Park et al., 2014; Thiele et al., 2009).

The evolutionary significance of callose deposition at the cytokinetic junction has received little attention, even though it is an essential component of cell division in land plants. Callose has been observed at the division plane of streptophycean algae including *Chara* and *Coleochaete,* and filamentous and/or branched chlorophycean algae (Scherp et al., 2001). Thus far, callose has only been reported at the cytokinesis junctions of multicellular plant species, leading to the hypothesis that callose is specifically associated with multicellularity in the green plant lineage (Scherp et al., 2001).

The lack of in-depth studies of cytokinetic callose in lineages closely related to land plants impedes our understanding of callose's role in the evolution of land plant cytokinesis and cell wall formation. A valuable model to investigate this question is *Penium margaritaceum*, a unicellular freshwater desmid of the Zygnematophyceae; the group of streptophytes that are most closely related to land plants (Delwiche and Cooper, 2015). *P. margaritaceum* has a simple cylindrical shape and consists of two semi-cells, each containing a multilobed chloroplast that surrounds a nucleus at the cell center, or isthmus (Rydahl et al., 2014). *P. margaritaceum* is valuable in cell biology studies because it is amenable to various live-cell-based methodologies used in microscopy-based and experimental analyses (Rydahl et al., 2014). Immunological studies of *P. margaritaceum* have shown that its cell wall composition is notably similar to that of the primary walls of land plants (Domozych et al., 2014; Sørensen et al., 2011), making it an ideal system to study the evolution of land plant cell wall formation. *P. margaritaceum* contains a cellulosic inner layer and two outer pectic layers that include rhamnogalacturonan-I (RG-I) and a distinct homogalacturonan (HG) lattice that covers the semi-cells, with the

[1]Department of Plant Sciences, University of California, Davis, Davis, CA 95616, USA. [2]Plant Biology Section, School of Integrative Plant Science, Cornell University, Ithaca, NY 14853, USA. [3]Department of Biology and Skidmore Microscopy Imaging Center, Skidmore College, Saratoga Springs, NY 12866, USA.

*Author for correspondence (gdrakakaki@ucdavis.edu)

M.W., 0000-0001-9545-7895; G.D., 0000-0002-3949-8657

Journal of Cell Science

1

notable exception of a narrow ring at the isthmus zone (Domozych et al., 2014), which is the site of wall polysaccharide deposition and assembly. The cell wall expands by the deposition of cellulose and pectin at the isthmus zone, which displaces older cell wall material towards the poles of the cell. The isthmus is also the site of pectin demethylesterification, with highly esterified HG being secreted first, followed by de-esterification and calcium binding to form the unique lattice (Domozych et al., 2014). The underlying cellular structure of the isthmus likely dictates the deposition and arrangement of new cell wall material. Identifying and characterizing events and structures at the isthmus zone is necessary to fully understand how *P. margaritaceum* grows and divides. By defining the events during *P. margaritaceum* cytokinesis we can begin to identify conserved cell wall features between later diverging land plants (i.e. embryophytes) and their aquatic ancestors.

In this study, we characterized cytokinesis in *P. margaritaceum*, with a focus on callose deposition during cell wall formation. This provided novel insights into the evolution of the land plant cell wall and cytokinesis strategies of this alga and helped clarify our understanding of cell division mechanisms employed by unicellular and multicellular plants.

RESULTS

Endosidin 7 treatment inhibits growth in *P. margaritaceum* cell cultures by disrupting cytokinesis

We took a pharmacological approach to dissect the role of callose in *P. margaritaceum* cytokinesis. In our previous studies, we identified and characterized endosidin 7 (ES7), a small molecule that specifically inhibits callose deposition during cytokinesis in land plants (Drakakaki et al., 2011; Park et al., 2014). We tested the effects of ES7 on cytokinesis in *P. margaritaceum*, and compared them with those previously observed in land plants. ES7 application inhibited *P. margaritaceum* growth in a concentration-dependent manner (Fig. 1A). Specifically, a reduction in cell culture optical density (a metric used to determine cell numbers) was observed upon treatment with ES7. The effect was first noticeable 4 days after ES7 application and was most apparent 7 days after treatment. In cultures supplemented with 5 μM ES7 for 7 days, cell numbers were reduced by ∼30% compared to those of the DMSO control, whereas cell numbers in cultures grown in 7.5 μM ES7 or 10 μM ES7 for 7 days decreased by ∼60% and ∼69%, respectively, in comparison to those in the DMSO control (Fig. 1A). An initial delay in the inhibitory action of ES7 likely reflects an acclimation period of the cells to new medium containing ES7 prior to reaching exponential growth. A similar acclimation period is seen in cycloheximide-treated cultures (Fig. S1). No significant differences were observed at any time point between *P. margaritaceum* cultures grown in growth medium alone (NT) or in medium containing the solvent (DMSO) employed to dissolve ES7.

After noting the inhibitory effect of ES7 on cell culture growth, we then investigated whether this was due to inhibition of cytokinesis, as previously shown in ES7-treated *A. thaliana* seedlings (Park et al., 2014). We recorded the presence of cytokinesis phenotypes in the 7-day ES7-treated *P. margaritaceum* cultures and subsequently focused our attention on the isthmus zone (Fig. 1B). After 7 days of 5 μM, 7.5 μM or 10 μM ES7 treatments, we observed a higher proportion of fused cells (binucleate cells connected by a thin cytoplasmic strand; Fig. 1B, yellow bars and corresponding microscopy image) and cells with atypically elongated isthmus zones when compared those of DMSO control cells (Fig. 1B, purple bars and corresponding microscopy image). We concluded that cells with elongated isthmus zones represented a recent inhibition by ES7

in early mitosis, whereas fused cells were those that had completed mitosis and had paused at cytokinesis due to the action of ES7. Fused cells always contained two daughter nuclei (Fig. 1B, representative microscopy image), indicating a defect in cytokinesis. In addition, fused cells were characterized by a thin cytoplasmic thread connecting the two daughter cells, typically with a deep septum at the division plane (Fig. 1B, arrowhead in the corresponding microscopy image). The fused cell phenotype was not observed in DMSO-treated cells, but constituted 5.3% of the cells treated with 5 μM ES7, 5.2% of the cells in 7.5 μM ES7 and 6.9% of the cells in 10 μM ES7 (Fig. 1B). Non-dividing interphase (single nucleus) cells in control (DMSO) and ES7 treatments were indistinguishable. Control DMSO-treated cells exhibited elongated isthmus zones in only 0.8% of cells, versus 24% of cells grown in 5 μM ES7, 21% of cells grown in 7.5 μM ES7 and 23% of cells grown in 10 μM ES7 (Fig. 1B).

We then applied a short-term (2 day), high concentration of ES7 (50 μM) to test the specificity of the inhibitor during cytokinesis in semi-synchronized cultures and the reproducibility of the cytokinesis defects observed in 7-day, 10 μM ES7-treated cultures. Fused, binucleate cells that were unable to separate were observed in 12% of cells treated with 50 μM ES7 for 2 days, compared to 0% of cells in DMSO (Fig. 1B). Cells with an elongated isthmus represented 3.5% of cells in ES7 compared to 0% of cells in DMSO (Fig. 1B,C). The elongated isthmus of treated cells was approximately three times longer (averaged across all three ES7 concentrations) than the narrow isthmus found in control DMSO-treated cells (Fig. 1C). Isthmus zones of recovered cells (ES7 washout followed by 48 h recovery in DMSO) were not significantly different from isthmus zones of DMSO control cells (Fig. 1C). We carried out all subsequent experiments with cells treated with 50 μM ES7 for 2 days (∼48 h), because this treatment allowed us to maintain a higher degree of cell cycle synchronization (Fig. 1B, green bar of 2 day DMSO treatment compared to green bar of 7 day DMSO treatment).

The cell phenotype and growth data showed that ES7 has a similar effect on dividing *P. margaritaceum* cells as on dividing *A. thaliana* root cells, that is, daughter cells are unable to complete cytoplasmic separation following mitosis, resulting in binucleate cells (Park et al., 2014). Taken together, our results support a potential evolutionarily conserved ES7-inhibited pathway that acts during cytokinesis and is common to *P. margaritaceum* and land plants.

Callose is present at the division plane of *P. margaritaceum*

Our previous studies have shown that ES7 causes cytokinesis defects in *A. thaliana* by specifically inhibiting the deposition of callose at the cell plate (Park et al., 2014). Given the cytokinesis defect observed in ES7-treated *P. margaritaceum* cells, we hypothesized that callose plays a similar role in cytokinesis in this unicellular alga, challenging the view that callose is only present at the cytokinetic junctions of multicellular plant species (Scherp et al., 2001). Additionally, given the rapid progression of cytokinesis in *P. margaritaceum* (Movie 1), we posited that if callose is indeed present, it would be deposited during a very narrow time interval during late cell division, which in turn would make it difficult to observe. By closely examining the isthmus zone during cell division we were able to detect callose using two independent methods: Aniline Blue fluorochrome (Fig. 2; Evans et al., 1984); and a monoclonal antibody with specificity for β-1,3 glucans (Fig. 3; Meikle et al., 1991). Callose was first apparent as a single ring at the isthmus zone of slightly elongated cells prior to mitosis (Fig. 2B), a likely indication of pending cell division (Ochs et al.,
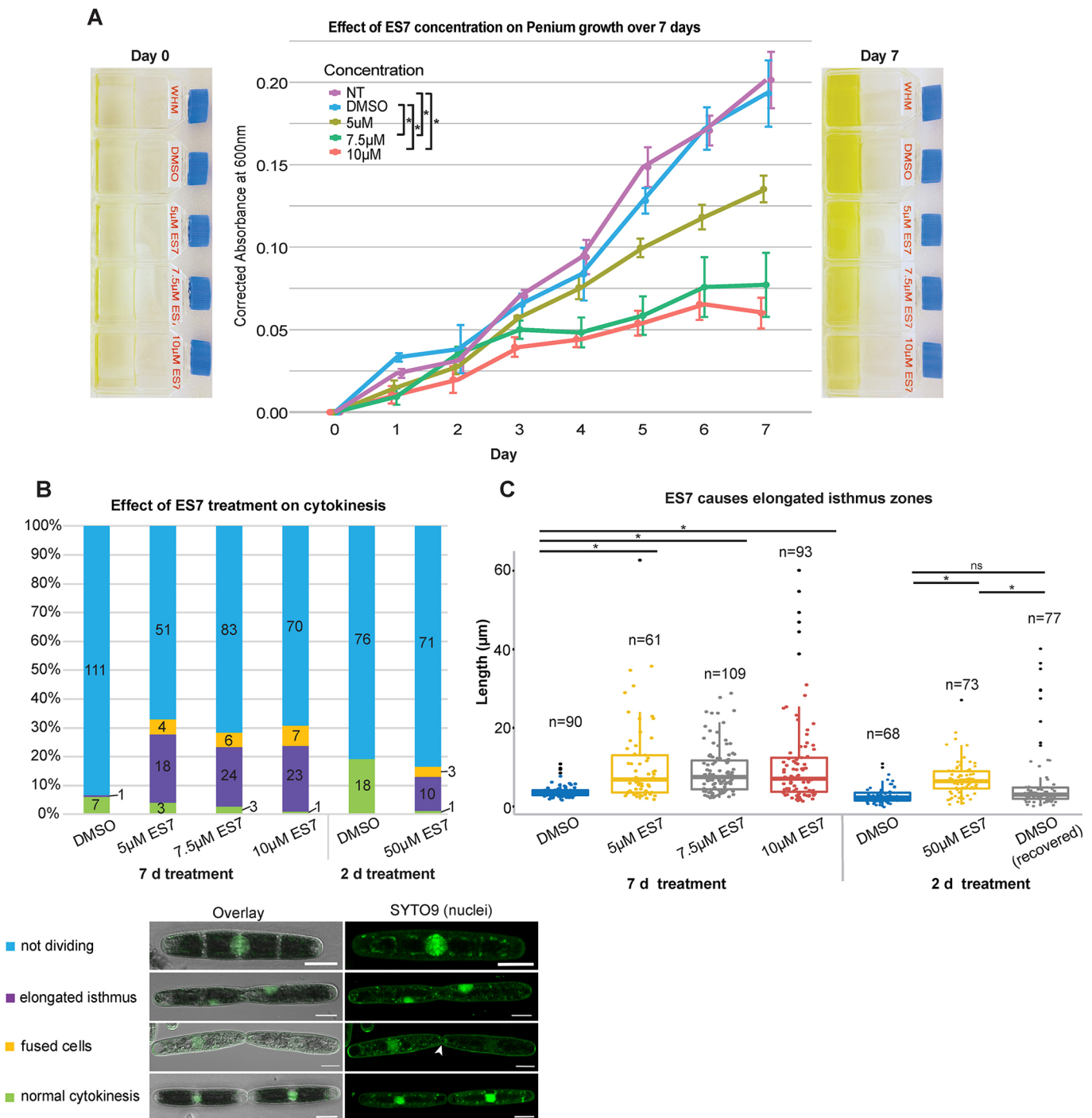
Fig. 1. ES7 treatment inhibits cell proliferation by disrupting cytokinesis in a concentration-dependent manner. (A) ES7 inhibition of *P. margaritaceum* liquid culture growth over a 7 day period measured by optical density (OD) at 600 nm. Data represent the mean±s.e.m. of three biological replicates, each measured three times per time point (technical replicates). *$P<0.05$ (one-way ANOVA with a Bonferroni correction). Representative images of day 0 and day 7 cultures are shown on each side of the graph. NT, growth medium alone. (B) Percentage of total cells exhibiting cytokinesis inhibition phenotypes in a series of low ES7 concentrations for 7 days and a 2-day high ES7 pulse treatment (numbers on bars indicate cell counts). Corresponding bright-field and nuclei-labeled (SYTO9) images are shown below. Scale bars: 20 µm. (C) Box plot of isthmus zone measurements of cells in the same ES7 treatments as stated for B, including measurements corresponding to ES7 washout and recovery in DMSO [DMSO (recovered)]. Boxes indicate the median and interquartile range. Whiskers show 1.5 times the interquartile range. Extreme outliers (black dots) were excluded from statistical analysis. *$P<0.05$; ns, not significant; 7-day and 2-day treatments measured by Welch's ANOVA test with Games–Howell post hoc test.

2014). We did not detect callose in interphase cells (Fig. 2A). Callose detection by Aniline Blue was more pronounced at the onset of cell division, with a bright Aniline Blue-labeled ring positioned at the isthmus zone while the nucleic acids were observed as a narrow

disk aligned at the isthmus (Fig. 2C). The single ring was maintained in cells with daughter nuclei at the isthmus zones of their respective daughter cells (Fig. 2D). In post-mitotic cells beginning cytokinesis, the single callose ring transformed into two
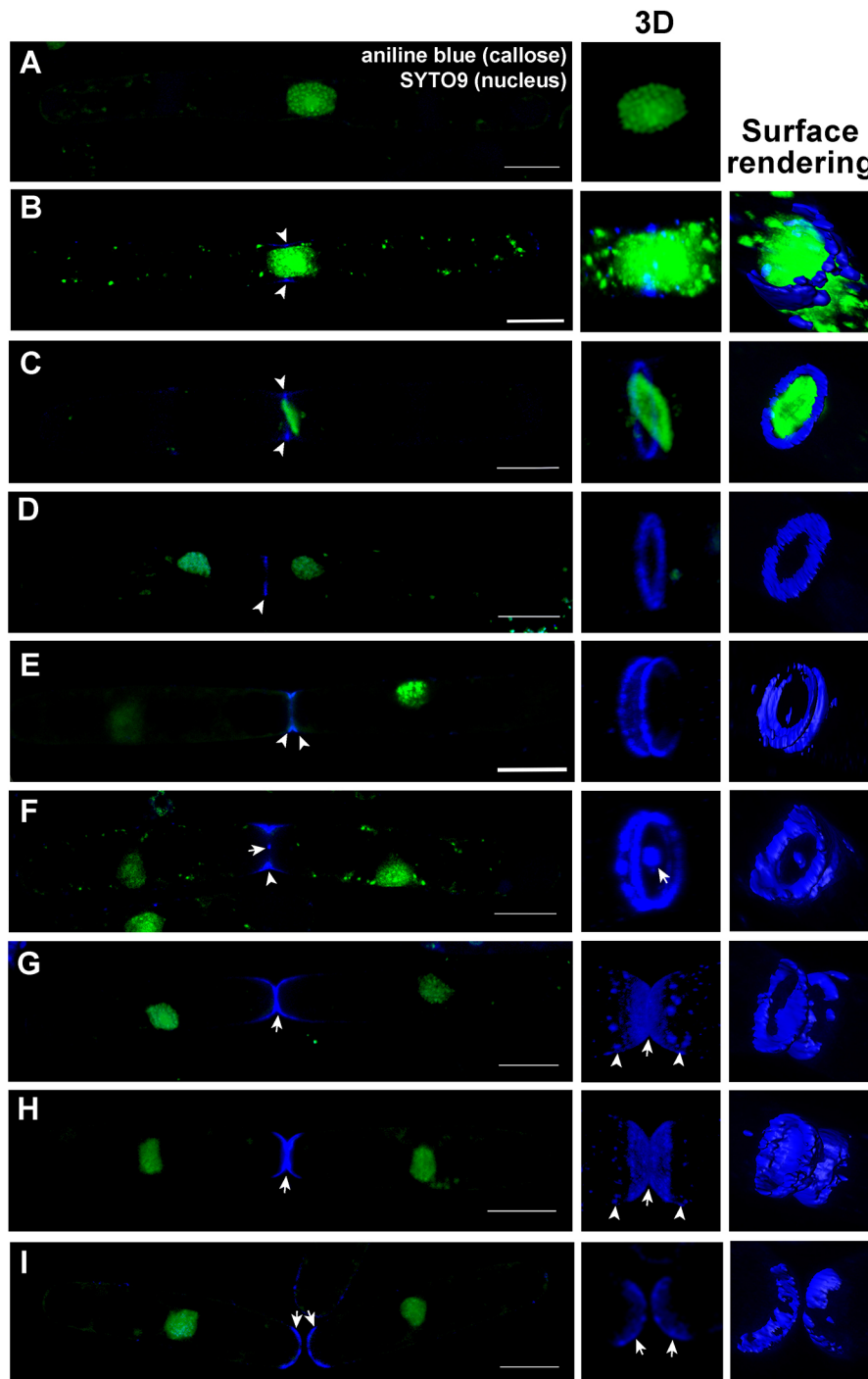
Fig. 2. Callose is deposited in distinct patterns at the division plane of *P. margaritaceum*. Callose deposition patterns labeled by Aniline Blue fluorochrome during different stages of cytokinesis in *P. margaritaceum*. Each panel is a distinct cell representing the Aniline Blue patterns observed during cytokinesis. (A) Interphase cells did not show callose deposition at the isthmus zone (*n*=26). (B–I) During the transition to mitosis, a single Aniline Blue-labeled ring was seen around the nucleus at the isthmus zone (B, arrowheads; *n*=9) that remained as the nucleus (SYTO9) collapsed into a disk (C, arrowheads; *n*=3) and persisted as daughter nuclei began migration to their respective isthmus zones (D, arrowhead; *n*=15). When daughter nuclei reached their isthmus zones, callose was observed as two rings (E, arrowheads; *n*=12). At the next stage, a bright Aniline Blue-labeled punctum (F, arrows) was present in the center of the two rings (F, arrowhead; *n*=5). During the ring disassembly stage (G, arrowheads), the punctum expanded and the isthmus zone constricted to form the daughter cell tips (G, arrows; *n*=9). The next stage is characterized by opposing callose caps at the poles of the dividing cells (H, arrows) and the disappearance of the callose rings (H, arrowheads; *n*=18). Callose caps remained until the daughter cells physically separated (I arrows; *n*=26). 3D images (center column) were produced using Zeiss Zen Black imaging software. Surface renderings shown to the right were produced using Imaris (Bitplane). Nuclei labeled by SYTO9 are shown in green; callose labeled by Aniline Blue fluorochrome is shown in blue. Scale bars: 20 µm.

rings [Fig. 2E, three-dimensional (3D) image and surface rendering]. As cell division progressed, cells exhibited two callose rings (Fig. 2F, arrowhead) surrounding a large Aniline Blue-labeled punctum (Fig. 2F, arrow). Subsequently, the punctum expanded throughout the two adjoining ends of the daughter cells (Fig. 2G, arrow) while the two callose rings (Fig. 2G, arrowheads) began to disassemble. Finally, Aniline Blue labeling appeared as 'caps' on the adjoining ends of the daughter cells (Fig. 2H, arrow) that remained for a period of time following the physical separation of the daughter cells (Fig. 2I). With these data we can summarize callose deposition into two general structures and associated stages: (1) callose ring(s) characteristic of early cytokinesis events; and (2) a callose punctum/caps characteristic of later cytokinesis events (Fig. 2, arrowheads and arrows, respectively). We also observed these representative structures and stages in dividing cells labeled with the anti-callose antibody (Fig. 3A). These results clearly demonstrate the presence of callose at the cytokinesis junction of a unicellular plant species, with a distinct deposition pattern in *P. margaritaceum*.

Callose deposition is essential for cytokinesis in *P. margaritaceum*

Given that ES7 arrested cell division in *P. margaritaceum* we investigated whether, like in *A. thaliana*, it inhibited callose
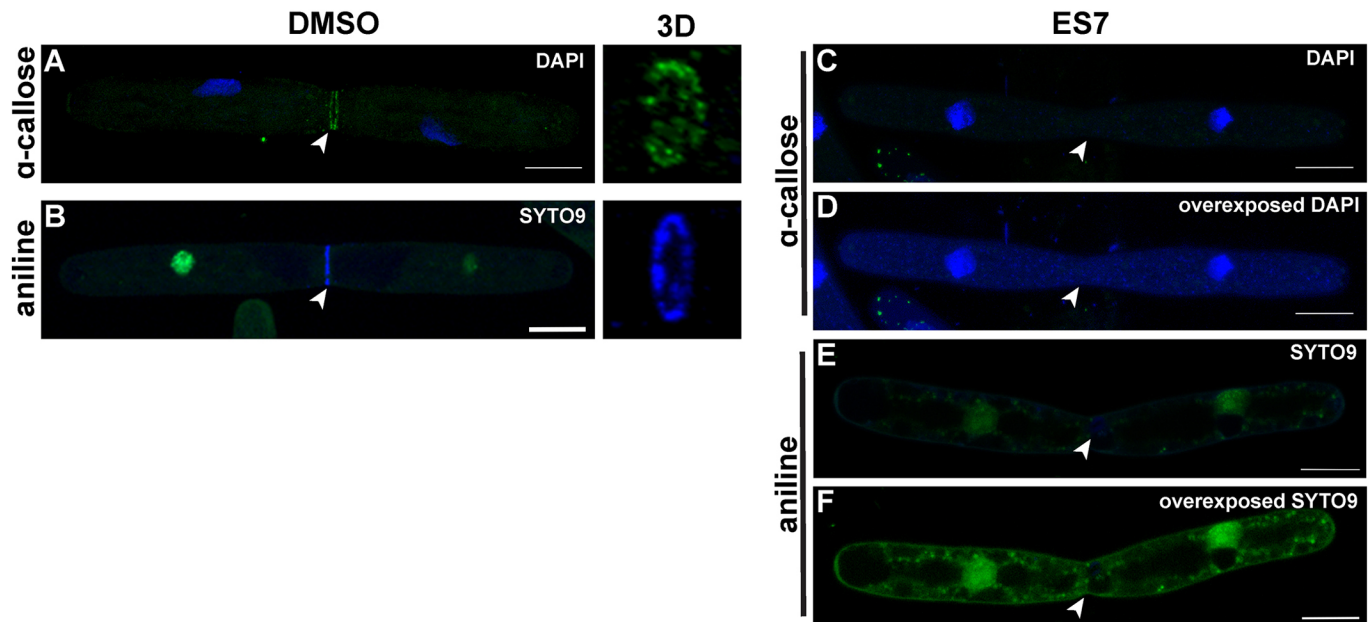
Fig. 3. Inhibition of callose at the isthmus zone leads to cytokinetic defects in *P. margaritaceum*. (A) Immunostaining of callose (α-callose, green) at the isthmus zone of dividing cells verifies the presence of the polymer (arrowhead; *n*=15). Nuclei are stained with DAPI (blue). (B) Immunolabeling of callose, as seen in A, mimicked the pattern observed with Aniline Blue fluorochrome (arrowhead, blue; *n*=15). Nuclei are stained with SYTO9 (green). (C–F) ES7 treatment inhibits callose deposition. The polymer is no longer detectable by callose antibodies (C,D; *n*=9) or Aniline Blue (E,F; *n*=20) at the isthmus zone of fused daughter cells (arrowheads) following ES7 treatment, visualized by overexposed fluorescence labeling of nuclei (D,F). Scale bars: 20 µm.

deposition at the division plane. In contrast to the callose rings observed in DMSO-treated control cells during early cytokinesis (Fig. 3A,B, arrowheads and 3D insets), no callose was detected, either immunologically or by Aniline Blue staining, in dividing cells treated with ES7 (Fig. 3C–F), mimicking the effect of ES7 treatment in dividing *A. thaliana* root tip cells (Park et al., 2014). This indicates that callose is required for the progression of cytokinesis and may suggest an evolutionarily conserved role for β-1,3 glucans during cell division among unicellular streptophyte algae and land plants.

Callose deposition is not essential for septum formation
A key difference between *P. margaritaceum* and land plants is the presence of a septum during cytokinesis (Pickett-Heaps et al., 1999). The *P. margaritaceum* septum manifests itself primarily as a curvature of the cell wall and constriction of the plasma membrane during the physical separation of daughter cells (Fig. 4A, arrowheads). Septum formation occurs at the isthmus and coincides with callose deposition (Fig. 4A,B). We sought to determine whether ES7 inhibits cell separation by disrupting septation. ES7 treatment did not alter the formation of the cell wall curvature and/or plasma membrane constriction that constitute the septum (Fig. 4C,D, arrowheads), even when callose was no longer detected (Fig. 4D–G), indicating that callose does not play a major role in septation.

The rapid series of events that occur at the division plane of *P. margaritaceum* (Movie 1) makes distinguishing septation from other cytokinesis components, including a potential cell plate, very difficult. Cytokinesis in the closely related multicellular zygnematophyte, *Spirogyra* sp., however, has been well characterized, including the processes of septation and cell plate formation (Fowke and Pickett-Heaps, 1969; Sawitzky and Grolig, 1995). Briefly, *Spirogyra* sp. initiates septum ingrowth from the cell wall during anaphase. The septum, containing fibrillar material and

surrounded by vesicles, then impinges upon the vacuole (Fowke and Pickett-Heaps, 1969). Notably, and in contrast to higher plants, in which microtubules serve as the primary cytokinetic vesicle and organelle 'tracks', septum growth in *Spirogyra* sp. is dependent on the microfilament cytoskeleton (McIntosh et al., 1995; Sawitzky and Grolig, 1995). Once the septum has bisected the parental cell halfway, a phragmoplast-like, microtubule 'basket' structure transforms to a cylinder as it makes contact with the ingrowing septum and forms the cell plate (Fig. 4O). Based on the presence of both a septum and a cell plate (guided by distinct cytoskeletons initially and their interaction for completion), *Spirogyra* sp. has been characterized as having an evolutionarily transitional form of cytokinesis (Fowke and Pickett-Heaps, 1969; McIntosh et al., 1995; Sawitzky and Grolig, 1995).

Taking advantage of this unique evolutionary position, we analyzed dividing *Spirogyra* sp. cells for the presence of callose and for an effect of ES7 treatment on cell division. *Spirogyra* sp. also deposited callose at the plane of division (Fig. 4H,I). Treatment of *Spirogyra* sp. cells with ES7 resulted in loss of callose, determined by the absence of Aniline Blue labeling (Fig. 4K,N), and disruption of cytokinesis, observed by the occurrence of binucleate cells and septum ingrowths (Fig. 4J and inset). Assuming that the curvature of the adjoining *P. margaritaceum* daughter cells is analogous to the septum in *Spirogyra* sp., our data suggest that ES7 does not significantly affect septum formation, but rather perturbs a callose-dependent process during cytokinesis, and in the case of *Spirogyra* sp., cell plate formation specifically (Fig. 4O).

Lack of callose alters the deposition pattern of polysaccharides during cell wall formation
The major polysaccharides in the mature cell wall of *P. margaritaceum* are cellulose and pectins, which are deposited at the isthmus and displace older cell wall components towards the two poles (Domozych, 2014; Domozych et al., 2007). Because the
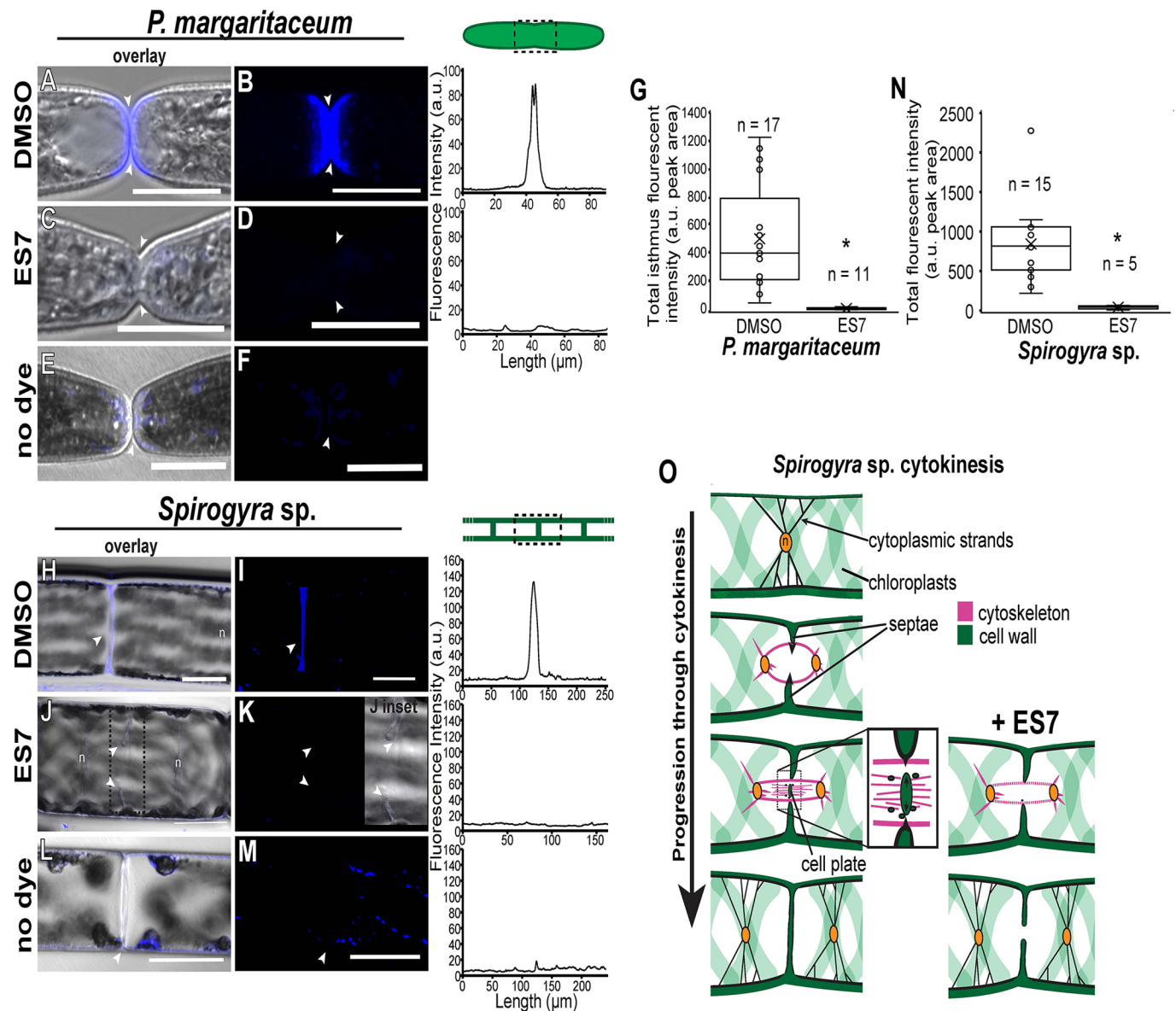
Fig. 4. ES7 treatment does not inhibit septum formation. Imaging of callose during divison of *P. margaritaceum* (A–F) and *Spirogyra* sp. (H–M) cells. Callose was detected by Aniline Blue fluorochrome (blue) at the division plane of *P. margaritaceum* (A,B; *n*=123) and *Spirogyra* sp. (H,I; *n*=39), coinciding with septum formation (arrowheads). Following ES7 treatment, callose was no longer detectable at the division plane of either species (D, *n*=29; K, *n*=5); however, septa characterized by isthmus zone constriction in *P. margaritaceum* (C, arrowheads; *n*=44) and membrane ingrowths in *Spirogyra* sp. (J and inset, arrowheads; *n*=5), were still visible in both species. Dashed lines in J indicate the region depicted in the enlarged inset, which shows formation of septum stubs (dashed outlines) despite the absence of callose. No-dye control images taken in the absence of Aniline Blue (E,F,L,M) indicate minimal off-target labeling. Dark-field images used in overlay panels are maximum intensity projections. Fluorescent intensity profiles are shown to the right of their corresponding images, with the measurement area (dashed box) graphically depicted above the graphs. (G,N) Boxplots of total Aniline Blue signal at the isthmus of *P. margaritaceum* (G) and the septum of *Spirogyra* sp. (N) following DMSO or ES7 treatment. Boxes indicate the median and interquartile range. Whiskers show the values outside the middle 50%. Asterisk indicates significant difference from cells treated with DMSO (*t*-test; *P*<0.05). (O) Schematic representation of cytokinesis in *Spirogyra* sp. and its inhibition by ES7. Scale bars: A–F, 20 μm; H–M, 50 μm. n, nucleus.

isthmus is the focal point of both callose deposition and the deposition of wall polymers, we assessed the impact of the lack of callose, due to ES7 treatment, on subsequent cell wall development. During interphase in both control and ES7 treated cells, homogalacturonan (HG), labeled by the monoclonal antibody (mAb) JIM5, showed a typical lattice pattern across the entire cell wall surface, with the exception of a narrow unlabeled band at the isthmus zone (Fig. 5A,B,E,F and corresponding graphs). As the cells elongated prior to division, the narrow unlabeled isthmus zone expanded to form a wider band (Fig. 5C,D, and W, DMSO asterisk).

However, in cells arrested in cytokinesis by ES7, JIM5 labeling was seen covering the isthmus zone between two fused daughter cells (Fig. 5G,H,W). While JIM5-labeled HG in the older areas of the cell wall (i.e. away from the isthmus zone) maintained a normal lattice-like appearance (Fig. 5H inset, arrow), JIM5 labeling of the elongated isthmus produced a weak fluorescence signal with no lattice (Fig. 5W, ES7 asterisk) and an irregular pattern (Fig. 5H and inset).

HG labeled by the mAb JIM7 (capable of binding HG with a higher proportion of methylester groups) was typically found
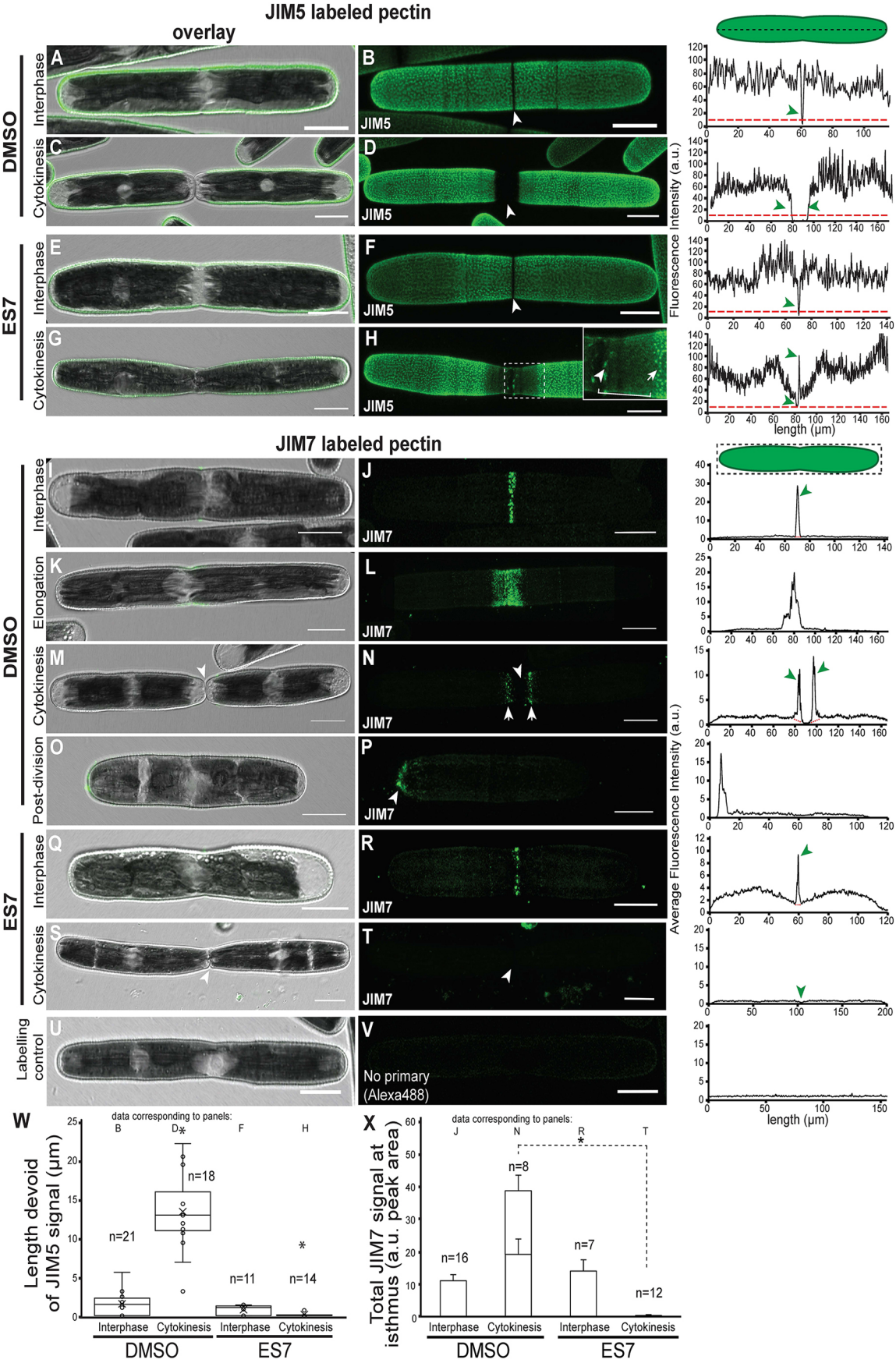
Fig. 5. See next page for legend.

Fig. 5. Pectin patterning changes in response to callose inhibition by ES7 treatment. (A,B) In DMSO-treated control cells during interphase, homogalacturonan (HG) labeled by JIM5 covered the entire cell surface in a regular lattice pattern, except for a narrow unlabeled ring at the isthmus (arrowhead; n=76). (C,D) During cytokinesis, the unlabeled isthmus ring from B expanded to a wide, unlabeled band (arrowhead; n=21). (E,F) ES7-treated interphase cells were indistinguishable from DMSO-treated control cells (n=54). Dividing cells treated with ES7, however, exhibited JIM5-labeled HG puncta in the isthmus zone (G,H; n=23; dashed box in H indicates region shown in inset). Notably, the normal JIM5 lattice pattern (H inset, arrow) was not maintained in the wall at the ES7-treated elongated isthmus (H inset, arrowhead and bracket). In contrast to JIM5, HG labeled by JIM7 antibodies was typically observed as a single narrow band at the isthmus zone (I,J) during interphase (n=13). During cell elongation prior to division, the JIM7-labeled HG band expanded (K,L; n=12) and eventually formed two distinct bands (arrows in N) on each side of the division plane (M,N; division plane marked by arrowhead; n=9). (O,P) Upon immediate physical separation of the daughter cells, JIM7 labeling remained at the new cell poles (arrowhead; n=4). (Q,R) JIM7-labeled HG in ES7-treated interphase cells was indistinguishable from that in DMSO-treated control cells (n=6). (S,T) During cytokinesis, however, JIM7 labeling was completely absent following ES7 treatment (isthmus of fused cell indicated by arrowhead; n=21). (U,V) Staining controls (no primary antibodies, Alexa Fluor 488 only). Fluorescence intensity profiles are shown to the right of the corresponding cell images. Green arrowheads indicate key fluorescent features corresponding to the white arrowheads (or for N, arrows) in the neighboring images. Measurement areas are graphically depicted above the graphs. (W,X) Quantification of JIM5 (W) and JIM7 (X) fluorescence signals in DMSO-treated control and ES7-treated cells during interphase and cytokinesis. Boxplot in W shows median and interquartile range. Whiskers show the values outside the middle 50%. Data in X are mean±s.e.m. Statistical significance was calculated by t-test. Asterisks in W indicate a significant difference from interphase cells treated with DMSO, and the asterisk in X indicates a significant difference between DMSO- and ES7-treated cells during cytokinesis. (*P<0.05). Fluorescence images are maximum intensity projections. Scale bars: 20 µm.

exclusively at the isthmus zone (Fig. 5I,J), consistent with previous observations (Domozych et al., 2011). Upon elongation, control cells exhibited a wide JIM7-labeled HG band at the isthmus zone (Fig. 5K,L), which later transformed into two distinct JIM7-labeled bands on either side of the division plane (Fig. 5M,N, arrows). Upon physical separation, the daughter cells retained JIM7 labeling at the once-connected cell poles, indicating continued cell wall maturation at the new cell poles (Fig. 5O,P). ES7-treated interphase cells showed no difference in JIM7 labeling compared to DMSO-treated control cells (Fig. 5I,J,Q,R,X). However, JIM7 labeling was absent from the isthmus zones of ES7-treated cells (Fig. 5X, asterisk) that exhibited a fused cell phenotype (Fig. 5S,T). DMSO-treated cells labeled with secondary antibodies (no primary) exhibited no detectable signal (Fig. 5U,V).

To gain a clearer view of cell wall dynamics and cytokinesis events during and following ES7 treatment, we combined cell wall labeling (JIM5) with ES7 washout, removing ES7 by washing cells with DMSO supplemented Woods Hole Medium (WHM), and observed cell wall growth and cytokinesis recovery. Cytochalasin E, a well-characterized inhibitor of actin polymerization, was used as a positive control of cytokinesis inhibition (Ochs et al., 2014). Following 48 h of recovery (from ES7 and cytochalasin E treatment) in fresh growth medium, cells exhibited normal JIM5-labeled HG deposition patterns of a lattice over the semi-cells with a narrow unlabeled isthmus zone that expanded to a large band during elongation (Fig. S2A,G,K). Comparing initial cell wall labeling (green) to new cell wall growth in recovery conditions (magenta) revealed that the majority of cells (ES7, 90.1%; cytochalasin E, 91.5%) elongated and/or divided normally (Fig. S2A–D, K–N compared to G–J). Some cells, however, retained ectopic JIM5-labeled HG in the isthmus zone and were devoid of new pectin

deposition at the daughter cell isthmus zones where elongation would occur (Fig. S2E,O), indicating no growth in recovery conditions. One cell following ES7 recovery and two cells following cytochalasin E recovery, however, deposited new cell wall both at the fused parental isthmus zone (for ES7 only) and the daughter cell isthmus zones, demonstrating cell wall growth despite the cytokinesis arrest (Fig. S2F and P, respectively). The presence of fused cells following recovery suggests that the deposition of callose during cytokinesis is a significant checkpoint in *P. margaritaceum* cell division, from which it never recovers once interrupted. Of note is the common JIM5 phenotype observed in ES7- and cytochalasin E-treated cells. Similar to the labeling in ES7-treated cells (Fig. 5H), JIM5-labeled HG is present in the elongated isthmus zone of cytochalasin E-treated cells (Fig. S2Q–V), even as callose remains present at the isthmus zone (Fig. S2S–X), illustrating a degree of specificity of ES7 to callose deposition.

Cellulose labeling with a carbohydrate-binding module specific to crystalline cellulose fused to green fluorescent protein (GFP–CBM3a) was observed as either one or two bright, narrow rings at the isthmus zone, consistent with previous observations (Fig. S3A–C; Domozych, 2014) The difference in signal intensities between the mature cell wall and the isthmus is likely due to easier access of the probe to the isthmus zone, because this region of the cell wall is devoid of mature pectin (Domozych, 2014). Although the typical GFP–CBM3a-labeled single ring was seen in ES7-treated fused cells (Fig. S3D,E), we also observed fused cells with multiple rings off-center from the isthmus zone (Fig. S3F), within the isthmus zone (Fig. S3G) or multiple rings near the isthmus zone (Fig. S3H).

In summary, cell wall polymer labeling showed that a lack of callose in the isthmus zone of dividing cells and the subsequent arrest of cytokinesis affects the deposition pattern of both cellulose and pectin specifically at the isthmus zone during cytokinesis. Additionally, these effects do not induce changes in the older cell wall. Our data further show that inhibition of cytokinetic callose does not affect the biosynthesis of structural polysaccharides, but likely influences the architecture of the isthmus zone, which may indirectly affect the polysaccharide deposition pattern.

Glucan synthase-like genes of *P. margaritaceum* are more closely related to those of land plants than to homologs in the Chlorophyta

Glucan synthase-like (GSL) proteins are enzymes that incorporate UDP-glucose into β-1,3 glucan and are responsible for callose deposition at the division plate in higher plants (Chen et al., 2009; Verma and Hong, 2001). Analysis by NCBI conserved domain search (Lu et al., 2019) of representative plant GSL proteins ranging from chlorophyte algae to *A. thaliana* revealed them to be large proteins of ∼2000 amino acids, consisting of the glucan synthase domain and the glucan synthase subunit FKS1 domain. In addition, the N-terminus regulatory domain, Vta1 is prevalent in land plant GSL proteins (Fig. S4).

The similar effects of ES7-treatment on cell division and callose deposition in *P. margaritaceum* and *A. thaliana* suggests that their respective GSL proteins have similar molecular properties. To identify candidate *P. margaritaceum* proteins, we searched the newly released *P. margaritaceum* genome assembly and transcriptome (Jiao et al., 2020) using BLAST analysis (Altschul et al., 1990) with the 12 *A. thaliana* GSL isoform sequences as the query. This revealed 15 putative full-length *P. margaritaceum* GSL proteins, four of which showed greater than 50% amino acid sequence similarity to AtGSL2 (also known as AtCALS5), an *A. thaliana* GSL with the glucan synthase domain, FKS1 domain

and the regulatory Vta1 domain (Fig. S4). The other eleven *P. margaritaceum* sequences showed less than 30% amino acid sequence similarity to AtGSL2 (Fig. S4). The four *P. margaritaceum* GSLs that showed greater than 50% amino acid similarity to AtGSL2 were used in subsequent phylogenetic analyses (Fig. 6, red asterisks).

A phylogenetic analysis of full-length GSL proteins from algae and land plants revealed that GSL proteins of chlorophyte algae (Fig. 6, orange) form an outgroup in an unrooted tree (Fig. 6, blue arrow), whereas GSL proteins of *P. margaritaceum* and *Klebsormidium flaccidum*, a multicellular charophyte, are more closely related to the GSL proteins of land plants (Fig. 6, black arrow). In the clade containing the *P. margaritaceum* GSL proteins pm0123640g0030, pm000009g0010 and pm010253g0010, all the land plants have at least one copy of a GSL homolog, suggesting that the land plants have homologs of ancestral charophyte GSL genes (Fig. 6, black arrow). Phylogenetic analysis of plant GSL proteins from the Chlorophyta, Charophyta, Bryophyta, Pteridophyta and Spermatophyta suggested that *P. margaritaceum* GSL proteins are more closely related to those from land plants than to those from chlorophyte algae.

DISCUSSION
Callose is deposited at the division plane of *P. margaritaceum* and is necessary for the completion of cytokinesis

Callose deposition in land plants is an essential component of cell wall formation during cytokinesis (Samuels et al., 1995). Without the tight temporal and spatial deposition of callose at the expanding cell plate, the transition of the cell plate to a nascent cell wall is arrested and daughter cells fail to separate, leading to binucleate cells (Chen et al., 2009; Guseman et al., 2010; Park et al., 2014; Thiele et al., 2009). It has been proposed that only multicellular species of plants take advantage of the unique elastic properties of callose during cytokinesis (Scherp et al., 2001). Given the wide variety of plant body phenotypes and the diverse array of transitional cytokinetic characteristics in the algal lineages most closely related to land plants, a key question remains as to whether callose deposition during cytokinesis is strictly a multicellular characteristic (Hall et al., 2008).

Our earlier studies established ES7 as a highly specific tool in dissecting the role of callose during cytokinesis in *A. thaliana* (Drakakaki et al., 2011; Park et al., 2014). Treatment of *P. margaritaceum* with ES7 has a similar effect on cytokinesis as in *A. thaliana*, leading to the formation of binucleate cells (Park et al., 2014). In land plants, it is hypothesized that callose plays an essential role in providing mechanical support of the cell plate and aids in its expansion (Jawaid et al., 2020 preprint; Samuels et al., 1995). Although a cell plate was not visible in our light microscopy experiments with *P. margaritaceum*, the clear inhibition of cytokinesis following ES7 treatment suggests that callose also has an essential function in *P. margaritaceum* cell division. Many details of the role that callose plays in the cell division of *P. margaritaceum* remain to be determined; however, the distinct temporal and spatial callose patterning and effects of ES7 treatment provide valuable insights. For example, the highly elongated isthmus zone observed in ES7-treated premitotic cells might reflect a role for callose in demarking the narrow area of the isthmus zone by maintaining the underlying isthmus zone structure. The occasional presence of a callose ring observed at the isthmus zone of premitotic cells (Fig. 2B) could support this hypothesis. It is unclear whether a callose ring

is a constant fixture of the isthmus zone or if it appears only in preparation for cytokinesis, given that it was not seen in every premitotic cell.

Distinct callose patterns characterize cytokinesis stages in *P. margaritaceum*

It was not until the onset of cytokinesis that callose was seen as temporally distinct, brightly labeled patterns by Aniline Blue staining; first as Aniline Blue-labeled rings, and later as Aniline Blue-labeled caps. Ringed callose always preceded the presence of callose caps and was the only callose pattern seen prior to migration of daughter cell nuclei. Because of this temporal separation, we can define early cytokinetic events as those with ringed callose and late cytokinetic events as having callose caps. The transition between these two patterns and stages of cytokinesis was also clearly distinguished by the appearance of the conspicuous central callose punctum between the two callose rings (Fig. 2E). In subsequent stages, the callose foci appeared to expand to form the caps while the two callose rings disassembled, visualized as Aniline Blue-labeled fragments (Fig. 2F). We propose that the distinct ring and cap callose deposition patterns have distinct functions but are both required for proper cell separation. Callose hydrogels, with their ability to associate with cellulose to reduce its rigidity (Abou-Saleh et al., 2018), are likely advantageous in covering the dome-shaped apex of dividing cells. Specifically, the elastic properties of callose hydrogels could provide a flexible barrier during separation while maintaining a curved shape at the new daughter cell poles. In addition, the callose dome itself might be the initial loadbearing support for the cell wall and provide a mechanism to overcome tension stress, as has been previously proposed for pollen tube growth (Parre and Geitmann, 2005). Evidence from aeroterrestrial algae, such as *Klebsormidium*, points towards a role for callose deposition in shoring-up areas of the cell wall prone to experiencing biomechanical stress due to loss of turgor pressure (Herburger and Holzinger, 2015). In this model, the elastic properties of callose enhance cell wall flexibility to a degree that is necessary for life in habitats with fluctuating water availability; a feature thought to be key for dispersal and to have led to the widespread success of these algae (Holzinger et al., 2015). The increased deposition of callose during water scarcity paired with the lack of typical load-bearing components of the cell wall and glycoproteins in *Klebsormidium* suggest that callose deposition might be an ancient mechanism for providing cell wall support in a variety of habitats and developmental stages.

Cytokinesis in *Spirogyra* sp. also occurs in distinct phases, as shown by chemical inhibition and physical disruption of cytoskeletal structures at specific time points (McIntosh et al., 1995). Specifically, depolymerization of phragmoplast microtubules was reported to inhibit complete cross-wall closure, while the septum was not affected, indicating that septation alone is not sufficient for the completion of cytokinesis (McIntosh et al., 1995; Sawitzky and Grolig, 1995). Our experiments here with ES7 treatments of *Spirogyra* sp. point to the same conclusion, in that inhibition of callose deposition (and, presumably, cell plate formation) resulted in cytokinesis defects but had no effect on septum initiation (Fig. 4J and inset). In that these two systems, one multicellular and one unicellular, employ comparable, transitional (with respect to evolution) structures to achieve cell division (i.e. septum and a cell plate) makes their comparison all the more interesting. The well-characterized cytokinetic events in *Spirogyra* sp. can lead to evolutionarily significant hypotheses regarding the role of
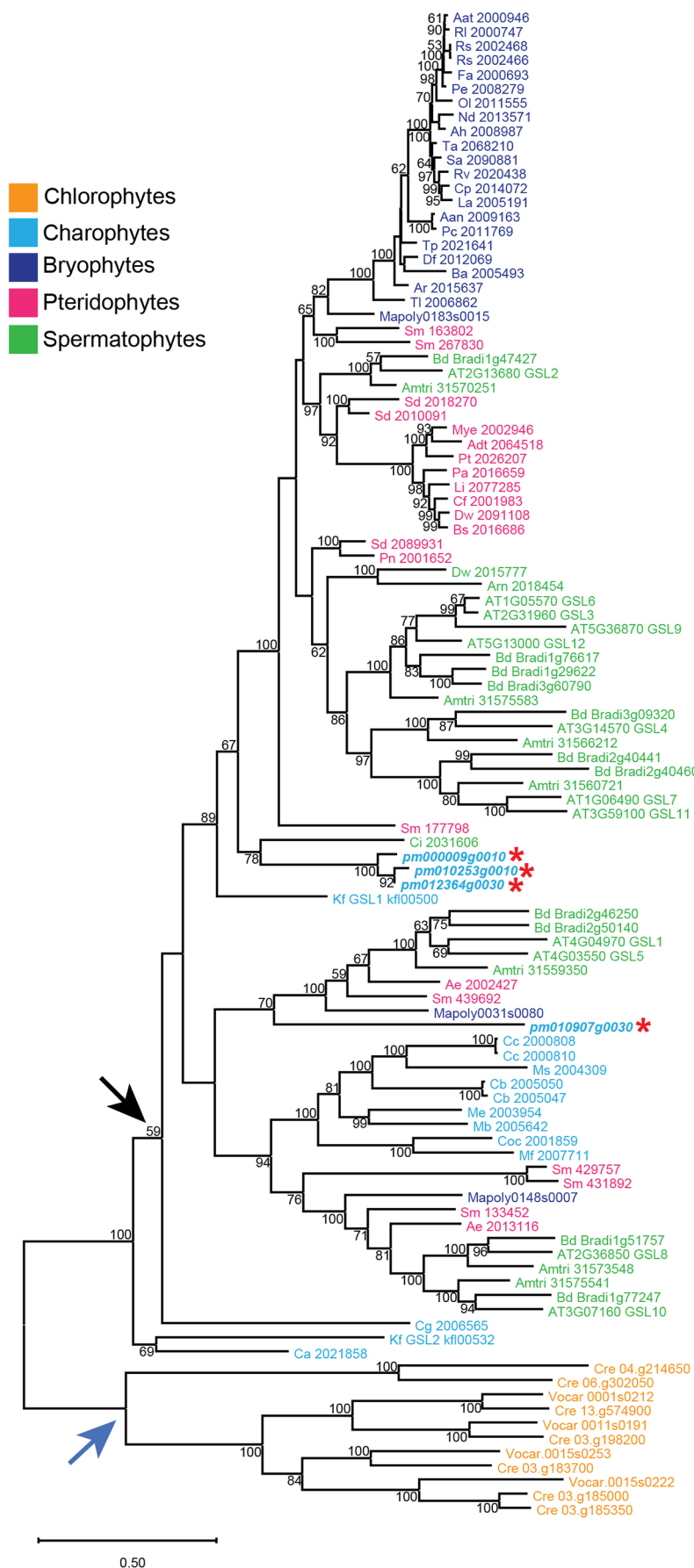
Fig. 6. Phylogenetic analysis of glucan synthase-like enzymes. GSLs of representative species of Embryophyta (including bryophytes, pteridophytes and spermatophytes), Charophyta and Chlorophyta were aligned using T-Coffee and analyzed in MEGA to construct unrooted maximum-likelihood trees of full length GSLs. Bootstrap values are labeled at each branch (branches with a bootstrap value below 50 are left unresolved) and evolutionary distance is proportionally drawn by branch length. Phytozome and 1KP project (db.cngb.org/onekp) accession numbers were used to name the enzymes, except *P. margaritaceum* sequences (asterisks) which were obtained from Jiao et al. (2020) and *Klebsormidium flaccidum* sequences obtained from the *Klebsormidium* genome project website. Text color corresponds to taxonomic group. Blue arrow indicates the early divergent branch of Chlorophyte GSL proteins; black arrow indicates the branch point of Charophyte and land plant GSL proteins. Aan, *Atrichum angustatum*; Aat, *Anomodon attenuatus*; Adt, *Adiantum tenerum*; Ae, *Angiopteris evecta*; Ah, *Aulacomnium heterostichum*; Amtri, *Amborella trichopoda*; Ar, *Andreaea rupestris*; Arn, *Argyrochosma nivea*; AT, *Arabidopsis thaliana*; Ba, *Buxbaumia aphylla*; Bd, *Brachypodium distachyon*; Bs, *Blechnum spicant*; Ca, *Chlorokybus atmophyticus*; Cf, *Cystopteris fragilis*; Ci, *Coleochaete irregularis*; Cg, *Chaetosphaeridium globosum*; Cre, *Chlamydomonas reinhardtii*; Coc, *Cosmocladium constrictum*; Cp, *Ceratodon purpureus*; Cb, *Cylindrocystis brebissonii*; Cc, *Cylindrocystis cushleckae*; Df, *Diphyscium foliosum*; Dw, Diplazium wichurae; Fa, *Fontinalis antipyretica*; Fv, *Frisvollia varia*; Kf, *Klebsormidium flaccidum*; La, *Leucobryum albidum*; Lb, *Loeskeobryum brevirostre*; Li, *Leucostegia immersa*; Mapoly, *Marchanita polymorpha*; Mb, *Mesotaenium braunii*; Me, *Mesotaenium endlicherianum*; Mf, *Micrasterias fimbriata*; Ms, *Mougeotia* sp.; Mye, *Myriopteris eatonii*; Nd, *Neckera douglasii*; Ol, *Orthotrichum lyellii*; Pa, *Polypodium amorphum*; Pc, *Polytrichum commune*; Pe, *Pseudotaxiphyllum elegans*; Pl, *Pulvigera lyellii*; pm, *Penium margaritaceum*; Pn, *Psilotum nudum*; Pt, *Pityrogramma trifoliata*; Rl, *Rhytidiadelphus loreus*; Rs, *Rhynchostegium serrulatum*; Rv, *Racomitrium varium*; Sa, *Scouleria aquatica*; Ta, *Timmia austriaca*; Tl, *Takakia lepidozioides*; Tp, *Tetraphis pellucida*; Sd, *Sceptridium dissectum*; Sm, *Selaginella moellendorffii*; Vocar, *Volvox carteri*. Evolutionary distance is proportionally drawn with branch length indicating the number of substitutions per site (scale bar at the bottom).

the actin and microtubule cytoskeletons during cytokinesis in *P. margaritaceum*. Of interest would be to assess whether *P. margaritaceum* also employs the actin and microtubule cytoskeletons differentially during cytokinesis.

Collectively, our data, consistent with findings for other zygnematophycean species (Ochs et al., 2014; Sawitzky and Grolig, 1995), suggest that cytokinesis in *P. margaritaceum* represents a transitional form of cell division that emerged prior to the first land plants. This hypothesis is based on several key pieces of evidence: (1) callose is essential for the completion of cytokinesis in land plants and both algae species observed in this study, and specifically for cell plate formation in *Spirogyra* sp. and *A. thaliana*; (2) in *P. margaritaceum*, the central callose punctum appears at the last physical location of daughter cell connection, where a cell plate is expected; and (3) the central callose punctum appears to expand centrifugally, as in *Spirogyra* sp. and land plants, in contrast to the centripetal growth of the septum.

The presence of the callose rings is intriguing. In fission yeast, enriched β-1,3 glucan deposition characterizes septum formation and is regulated by the activity of specific glucan synthases (Cortés et al., 2016). In dividing yeast cells, callose is deposited in the secondary septum once the chitin-rich primary septum has developed (Fraschini, 2020). Our study showed that septum formation is still achieved in the absence of callose, as evidenced by the clear furrows of ES7-treated *Spirogyra* sp. and *P. margaritaceum* (Fig. 4). Therefore, we hypothesize that callose aids in supporting the membrane as it grows inward during new daughter cell pole formation in cytokinesis but is not required for septum initiation. The highly elongated and fused isthmus zones of ES7-treated cells is consistent with this idea. A role of callose in supporting septum formation shared between yeast and *P. margaritaceum* could indicate evolutionary conservation across eukaryotes.

Callose inhibition during cytokinesis may affect cell wall polysaccharide assembly by perturbing isthmus zone architecture

The isthmus zone of *P. margaritaceum* is a highly dynamic area of the cell wall. Not only is it the location of division, but it also marks the area of new cell wall deposition and assembly at all stages of the cell cycle (Domozych et al., 2011). During cell wall growth, pectin incorporation follows a consistent sequential pattern beginning with the deposition of highly esterified HG, followed by cell wall displacement, de-esterification and calcium crosslinking. We hypothesize that highly esterified HG is deposited at the isthmus zone and, only in the final stages of cytokinesis, at a location interior to the isthmus zone, where it grows outward centrifugally, as a cell plate would grow, to eventually cover the newly separated daughter cell poles. As stated previously, we hypothesize that the central callose punctum marks the presumed cell plate in dividing *P. margaritaceum* cells. However, further experimentation involving high-resolution microscopy is necessary to identify the callose punctum as a cell plate and elucidate polysaccharide deposition dynamics interior to the isthmus zone. Whether, and in what form, pectin deposition occurs at the callose punctum is of particular interest given the role pectin plays in adhesion of plant cells (Daher and Braybrook, 2015).

It was apparent from our studies that, while the older cell wall was not affected by ES7-mediated cytokinesis inhibition, the wall at the isthmus zone was more susceptible to changes. Dividing cells treated with ES7 could compensate for the lack of callose by either synthesizing an excess, or directing the deposition of polysaccharides

such as cellulose and pectin to the isthmus zone (Fig. 5H, inset; Fig. S3). The loss of the normal JIM5-labeled lattice pattern together with the presence of weak and or aberrant JIM5 labeling in the isthmus might represent an effect on the underlying structure of the isthmus zone during cytokinesis, as a consequence of the loss of callose following chemical treatment. It is plausible that the lack of callose changes some conformational component at the isthmus so that the deposition pattern of HG is disrupted (Domozych et al., 2014). Additionally, due to other unknown mechanisms of action of ES7, it is possible that ES7 disrupts the delivery and deposition of cell wall material, in general.

Increases in HG deposition with a low level of esterification paired with increases in calcium crosslinking to compensate for the loss of another cell wall polysaccharide, such as cellulose, is a common feature of cell wall plasticity (Díaz-Cacho et al., 1999; Manfield et al., 2004; Sabba et al., 1999; Shedletzky et al., 1990). The absence of callose during cytokinesis may lead to the deposition of the predominant wall polymer in *P. margaritaceum*, namely partially esterified HG (Domozych et al., 2007), strengthening linkages with calcium ions and stabilizing the isthmus zone. This is probably achieved by an increase in pectin methylesterase activity at the isthmus zone in response to the inability to separate. The lack of HG labeled by JIM7 in ES7-treated cells points to a similar conclusion (Fig. 5T). Our recovery experiments also revealed cells that were unable to divide even after ES7 washout (Fig. S2E,F), indicating the presence of a checkpoint that, when disrupted, prevents the cell from progressing through cytokinesis.

Notably, we saw no obvious effect following ES7 treatment on any of the tested cell wall polysaccharides other than at or near the isthmus zone of dividing cells, highlighting the specific action of ES7 and, potentially, the role of callose in *P. margaritaceum*. In addition, polysaccharide deposition was always maintained in a ring-shaped pattern, suggesting that targeted secretion mechanisms of polysaccharides are likely not altered by ES7 treatment, consistent with our observations in *A. thaliana* (Drakakaki et al., 2011; Park et al., 2014).

Evolutionary insights into cytokinetic callose and putative callose synthase proteins in *P. margaritaceum*

Callose is involved in many physiological processes, including response to wounding, regulation of intercellular transport through plasmodesmata, pollen tube growth, cell wall reformation in protoplasts and cell plate formation (Piršelová and Matušíková, 2013). Interestingly, wound-induced callose deposition has been observed across evolutionarily distinct taxa, including unicellular chlorophyte algae, filamentous streptophyte algae and land plants (Jacobs et al., 2003; Scherp et al., 2001; Stone and Clarke, 1992). This is consistent with the presence of a number of callose synthases in the genomes of a wide range of plant species from chlorophytes to embryophytes (Fig. 6; Drábková and Honys, 2017; Ulvskov et al., 2013; Verma and Hong, 2001). The presence of callose at division planes appears to be a more recent evolutionary feature, having only been seen in multicellular species (both earlier and later diverging species relative to the land plant–Zyngematophyceae branch point). The presence of callose in *P. margaritaceum* likely reflects an evolutionary remnant from a multicellular ancestor that utilized callose in cytokinesis. The unicellular and filamentous Zygnematophyceae are thought to be derived from a morphologically complex ancestor (de Vries and Archibald, 2018; Delwiche and Cooper, 2015). The remarkable morphological reduction paired with the wide diversity of cell

division patterns in the Zygnematophyceae probably aided in the evolution of terrestrial plant life, in that simpler body plans are better able to survive rapidly changing habitats and variable water availability (Delwiche and Cooper, 2015; Hall et al., 2008).

Analysis of the *P. margaritaceum* genome (Jiao et al., 2020) revealed the presence of putative callose synthases. Phylogenetic analysis indicated that they have a closer relationship to homologs from land plants than to those from chlorophytes. The identification of putative callose synthases in *P. margaritaceum* supports the presence of callose as demonstrated by the immunodetection and pharmacological inhibition reported in this study. An important next step is to determine the *P. margaritaceum* isoform(s) responsible for callose deposition at the isthmus zone using complementation. However, although genetic transformation has been reported for *P. margaritaceum* (Sørensen et al., 2014), currently no complementation system has been reported.

Based on our results, we present a model of cytokinesis in *P. margaritaceum* (Fig. 7) that includes an essential role for callose in the final stages of cell division. This represents an important advance in our understanding of the evolutionary significance of cytokinetic callose – one that includes a unicellular plant species. Whether *P. margaritaceum* is an isolated example of a unicellular algae using callose during cytokinesis, or if other examples among the unicellular streptophyte algae exist, remains to be determined. Detailed studies to identify the role of cytokinetic callose in early diverging plant lineages are crucial in order to fully grasp the significance of its deposition in the evolution of land plant cytokinesis and cell wall assembly, particularly in the context of the migration of plants onto land.

MATERIALS AND METHODS
Growth and synchronization of cells

Penium margaritaceum (SKD-8 isolate, Skidmore College Algal Culture Collection) was maintained in liquid Woods Hole Medium (WHM) (Nichols, 1973) supplemented with 1.5% (v/v) soil extract (Carolina Biological Supply, Burlington, NC, USA), as previously described by Domozych et al., 2007. Cells were maintained in 30-ml cultures in vented Falcon culture flasks (Fisher Scientific, Hampton, NH, USA). Cells were subcultured weekly by diluting 3 ml of 7–14 day log-phase cultures to 27 ml of fresh WHM. *P. margaritaceum* cultures were grown in ambient temperature (~20–22°C) in an LED-lit cabinet with a photoperiod of
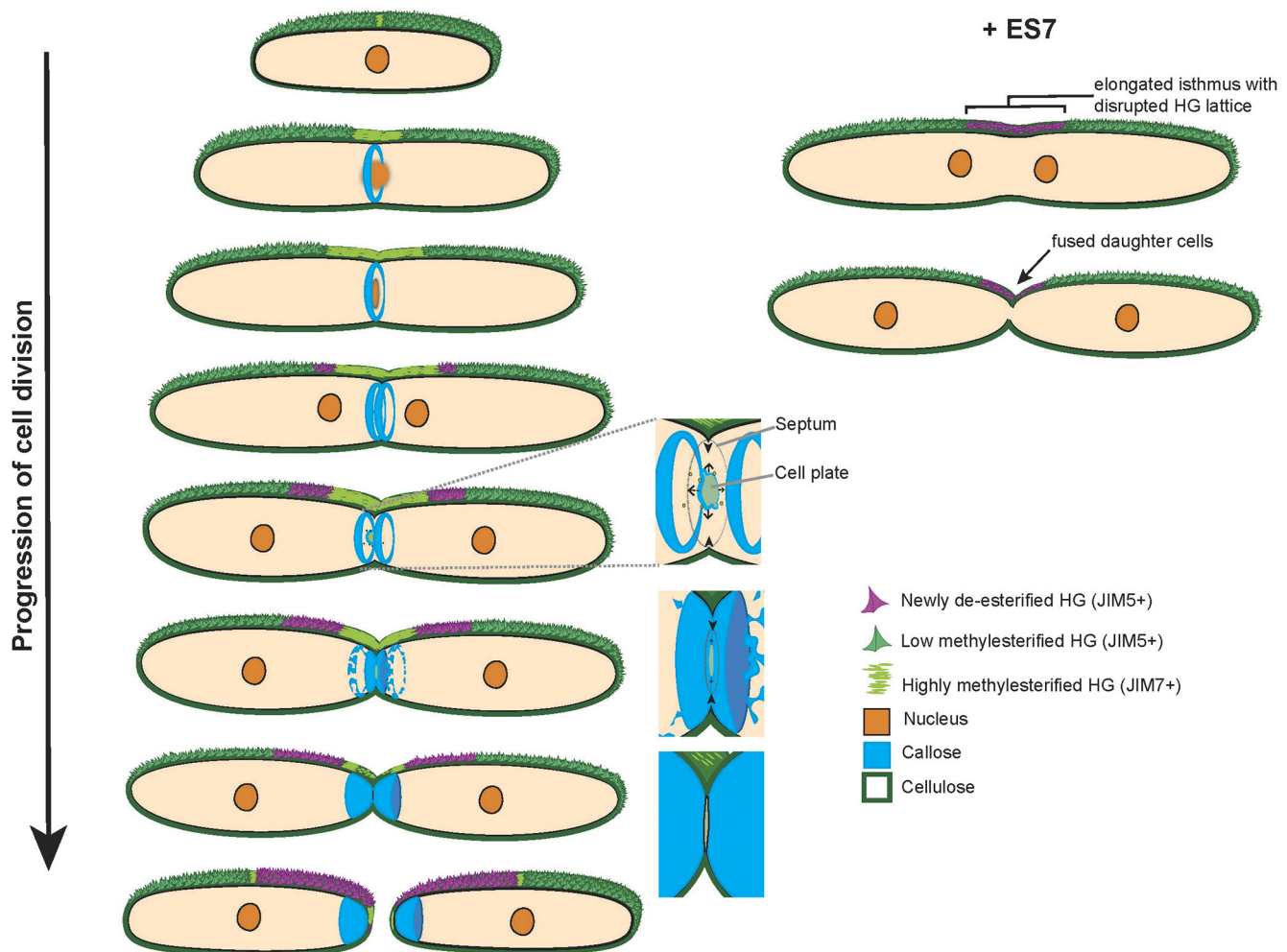

Fig. 7. Model of cytokinesis in *P. margaritaceum*. Dividing *P. margaritaceum* cells first deposit callose in a single ring prior to daughter nuclei formation. As cytokinesis progresses, the single callose ring transforms into two rings prior to the appearance of a central callose punctum that we hypothesize marks the cell plate. Pectin deposition at the isthmus continues during this process, with lattice formation (JIM5+) following the secretion of methylesterified HG (JIM7+), de-esterification and calcium crosslinking. The callose-rich (putative) cell plate then expands outward to meet the ingrowing septum. Once the cell plate meets the septum, cell wall formation continues with the deposition of cellulose and pectin to form two daughter cell poles. ES7 treatment (+ES7) disrupts the deposition of callose at the isthmus, which inhibits cytokinesis and causes elongation of the isthmus zone and formation of fused cells. The lack of callose during cytokinesis subsequently disrupts the normal HG lattice formation.

12 h. Cell synchronization was achieved within 4 days after subculture in new medium.

Spirogyra sp. (Carolina Biological Supply) was maintained in 3N-BBM (Andersen, 2005; Bischoff and Bold, 1963; Starr and Zeikus, 1993) in ambient temperature and light conditions. New subcultures were made every 2 weeks by adding several filaments to new medium.

Chemical treatment

P. margaritaceum: Log-phase *P. margaritaceum* cells were washed three times with fresh WHM and the pellet was resuspended in WHM supplemented with the indicated concentration of endosidin 7 (ES7; ChemBridge Corporation, San Diego, CA, USA) of either 5 µM, 7.5 µM, 10 µM or 50 µM diluted in DMSO. DMSO-treated control cells were cultured in WHM supplemented with an equal volume of DMSO alone. *P. margaritaceum* cells were grown for 48 h in the respective medium in the same light conditions as stated above prior to labeling and imaging.

Spirogyra sp.: For each treatment, three or more filaments of *Spirogyra* sp. were collected in a microcentrifuge tube with a sterile bacterial loop and washed three times with 3N-BBM by alternating light vortexing and pipetting. The filaments were added to fresh medium supplemented with DMSO or 50 µM ES7 and allowed to grow for 48 h prior to labeling and imaging.

For cytochalasin E (Sigma-Aldrich, Darmstadt, Germany) treatment, *P. margaritaceum* cells were collected and washed as before. Washed cell pellets were resuspended in 5 µg ml^{-1} cytochalasin E and grown for 48 h prior to labeling and imaging.

For cycloheximide treatment (Fisher Scientific, Waltham, MA, USA), *P. margaritaceum* cells were collected and washed as before. Washed cell pellets were resuspended in 30 ml fresh WHM supplemented with either 1 µg ml^{-1} or 10 µg ml^{-1} cycloheximide and grown for a total of 4 days.

Cell culture analysis

Cell culture absorbance at a wavelength of 600 nm was measured every 24 h with a Shimadzu spectrophotometer (UV-1700, Shimadzu, Kyoto, Japan), while WHM was used as control. ES7 phenotyping was carried out by observation of treated and non-treated cells under bright-field (BF) microscopy. Isthmus zone length was measured using BF images of *P. margaritaceum* cells and the line tool in FIJI (Schindelin et al., 2012).

Live-cell labeling and analysis

ES7- and control-treated *P. margaritaceum* cells were collected by centrifugation (2000 *g*, 1 min) and washed three times in WHM. Cells were resuspended in a 1:1000 dilution of SYTO9 (Invitrogen, Carlsbad, CA, USA) in water and vortexed for ~30 s to label nuclei. Cells were then washed once with water, and pellets were resuspended and incubated in 500 µl of a 1:40 (v/v) dilution of Aniline Blue fluorochrome (Biosupplies, LaTrobe University Melbourne, Australia) in water. Cells were incubated in Aniline Blue fluorochrome for 10 min at room temperature in the dark. Cells were then mounted on slides for imaging. For labeling *Spirogyra* sp. filaments, the ES7 or DMSO medium was removed by pipetting, and the filaments were labeled with Aniline Blue fluorochrome as described above for *P. margaritaceum*.

Live-cell immunolabeling and analysis

Prior to immunolabeling, *P. margaritaceum* cells (treated and control) were washed three times in fresh WHM, then HG immunolabeling was carried out as previously described in Domozych et al., 2011 and Worden et al., 2015. Briefly, 3 ml of treated or control cells were collected by centrifugation, washed three times with fresh WHM and blocked with 1% (w/v) powdered milk (Signature select, Pleasanton, CA, USA) for 20 min. The cells were then washed and labeled with the respective primary antibody for 1.5 h and washed and blocked again prior to labeling with the secondary antibody at room temperature in the dark. During recovery experiments, cells were first treated as described above, then washed six times with DMSO-supplemented WHM, and grown for 2 days prior to relabeling with JIM5 antibodies. The cell wall-directed antibodies were diluted in fresh WHM at the following concentrations: 1:10 dilution of rat-derived JIM5 directed against low methylesterified pectin (PlantProbes,

University of Leeds, Leeds, UK) and 1:8 dilution of JIM7 directed against highly methylesterified pectin (rat-derived, PlantProbes). Anti-rat Alexa Fluor 488 (Invitrogen) diluted to 1:50 (in WHM) was used as the secondary antibody for both JIM5 and JIM7. After the 2-day recovery, 1:50 anti-rat TRITC (Invitrogen) was used as the secondary antibody to distinguish new cell wall growth from previous growth.

Fixed-cell polysaccharide labeling

Cellulose was labeled with GFP–CBM3a (family 3 carbohydrate binding module; NZYtech, Lisboa, Portugal) following fixation with 1.5% paraformaldehyde (Electron Microscopy Sciences, Hatfield, PA, USA) plus 0.5% glutaraldehyde (Ted Pella, Redding, CA, USA) at room temperature for 20 min. Cells were then incubated in 1:2000 pectate lyase from *C. japonicus* (in WHM; Megazyme) for 20 min prior to washing and incubation with 1:200 GFP–CBM3a (in WHM containing 0.1 % Tween-20) for 90 min. Cells were then washed and counterstained with DAPI prior to imaging.

Callose labeling was performed by freeze shattering the cells and subsequent cell wall permeabilization, as previously described in Wasteneys et al., 1997. Briefly, ES7-treated and control-treated cells were collected by centrifugation, washed three times with fresh WHM and fixed in 1.5% paraformaldehyde (Electron Microscopy Sciences)+0.5% glutaraldehyde (Ted Pella) in 1× phosphate-buffered saline buffer (PBS) for 30 min at room temperature. The cells were centrifuged at 2000 *g*, and the resulting pellet was resuspended in ~15 µl, making a dense suspension that was sandwiched between two microscope slides and frozen by liquid nitrogen prior to shattering. Freeze shattered cells were washed into microcentrifuge tubes and subjected to a series of incubations and washes with permeabilizing buffers before being incubated with primary antibodies overnight at 4°C. Labeling was conducted as previously described in Ochs et al., 2014, with 1:1000 anti-callose primary antibody (mouse-derived, Biosupplies). Callose antibody-labeled cells were then incubated with 1:500 anti-mouse Alexa Fluor 488-conjugated secondary antibody (Life Technologies) in the dark for 1.5 h prior to final washing. Cells were counterstained with DAPI to visualize the nucleus and mounted on slides.

Microscopy

All microscopy was conducted using a 710 Zeiss Axio inverted Observer.Z1 laser scanning confocal microscope (Carl Zeiss AG, Oberkochen, Germany). The following settings were used to image the corresponding dyes and antibodies: Aniline Blue fluorochrome, 405 nm excitation laser at 2% intensity, emission 410–502 nm; SYTO9, 488 nm excitation laser at 2% intensity, emission 500–567 nm; GFP–CBM3a, 488 nm excitation laser at 10% intensity, emission 493–557 nm; Alexa Fluor 488, 488 excitation laser at 5% intensity, emission 493–630 nm, used as secondary antibody for anti-callose, JIM5 and JIM7 experiments – with the exception of the ES7 recovery experiments in which TRITC secondary antibodies were used (561 nm excitation laser at 2% intensity, emission 566–601 nm). All *P. margaritaceum* images were collected with Plan-Apo 40× (water, 1.1 NA) and 60× (oil, 1.4 NA) objectives. *Spirogyra* sp. images were collected with Plan-Apo 20× (air, 0.75 NA) and 40× (water, 1.1 NA) objectives. Image analysis and figure preparation was conducted using Zen Black and Blue (Zeiss) imaging software, Adobe Photoshop and Illustrator. Surface rendering of fluorescence images was performed using Imaris (BitPlane, South Windsor, CT, USA). Time-lapse acquisition of *P. margaritaceum* isthmus zone during cytokinesis under standard bright-field fluorescence microscopy was recoded for a period of 16 min.

Fluorescence intensity quantification

To quantify JIM5–Alexa Fluor 488 signal (Fig. 5), coordinates of fluorescence intensity along the longitudinal central axis of each *P. margaritaceum* cell were measured in FIJI ImageJ (Schindelin et al., 2012) using the segmented line function. Coordinates generated by FIJI ImageJ were used as the input for a MATLAB program (https://github.com/wangminmin777/Penium_JIM5/blob/master/cell_gap_calculation.txt) that measured the width of the region with no JIM5–Alexa Fluor 488 signal, with the threshold of fluorescence intensity set to 10 (~10% of maximum intensity).

13

To quantify JIM7–Alexa488 signal (Fig. 5) among different stages and treatments, average fluorescence intensity across the entire cell was measured using the rectangular selection tool in FIJI ImageJ. Peak area under the curve was used to compare total fluorescence signal at the isthmus zone of cells at interphase and cytokinesis. *P. margaritaceum* and *Spirogyra* sp. cells treated with DMSO and ES7 and stained with Aniline Blue (Fig. 4) were similarly quantified.

Phylogenetic analysis and tree construction

Previously characterized *Arabidopsis thaliana* GSL1–GSL12 (Dong, 2004; Chen and Kim, 2009) sequences were used as queries for a BLAST search against representative genomes of different groups of Embryophyta, Charophyta and Chlorophyta accessed at Phytozome 12 (phytozome.jgi. doe.gov/pz/), 1KP project (db.cngb.org/onekp) and the *Klebsormidium* genome project (plantmorphogenesis.bio.titech.ac.jp). The proteome database of *P. margaritaceum* was provided by Jiao et al., 2020, available at the Penium Genome Database (http://bioinfo.bti.cornell.edu/cgi-bin/Penium/home.cgi). GSL homologs showing over 50% amino acid sequence similarity against the queries with E-values lower than 1×10^{-17} were included in the analysis. Full-length GSL protein sequence alignment was performed using T-Coffee (Notredame et al., 2000), and was used as the input for unrooted phylogenetic tree construction with Mega 10 (Kumar et al., 2018) using the maximum-likelihood method and 1000 bootstrap replication. Analysis was performed with default settings in MEGA 10 with the partial deletion site coverage set to 50%.

Author contributions
Conceptualization: D.J.D., G.D.; Methodology: D.J.D., I.S., D.S.D., G.D.; Investigation: D.J.D., M.W., G.D.; Resources: J.K.C.R., I.S., D.S.D.; Writing - original draft: D.J.D., G.D.; Writing - review & editing: D.J.D., J.K.C.R., D.S.D., G.D.; Visualization: D.J.D.; Supervision: G.D.; Funding acquisition: G.D.

References
Abou-Saleh, R. H., Hernandez-Gomez, M. C., Amsbury, S., Paniagua, C., Bourdon, M., Miyashima, S., Helariutta, Y., Fuller, M., Budtova, T., Connell, S. D. et al. (2018). Interactions between callose and cellulose revealed through the analysis of biopolymer mixtures. *Nat. Commun.* 9, 1-13. doi:10.1038/s41467-018-06820-y

Altschul, S. F., Gish, W., Miller, W., Myers, E. W. and Lipman, D. J. (1990). Basic local alignment search tool. *J. Mol. Biol.* 215, 403-410. doi:10.1016/S0022-2836(05)80360-2

Andersen, R. A. (2005). *Algal Culturing Techiniques*. Elsevier Academic Press.

Balasubramanian, M. K., Bi, E. and Glotzer, M. (2004). Comparative analysis of cytokinesis in budding yeast, fission yeast and animal cells. *Curr. Biol.* 14, R806-R818. doi:10.1016/j.cub.2004.09.022

Bischoff, H. W. and Bold, H. C. (1963). *Some Soil Algae from Enchanted Rock and Related Algal Species*. Austin Tex: University of Texas.

Buschmann, H. and Zachgo, S. (2016). The evolution of cell division: from streptophyte algae to land plants. *Trends Plant Sci.* 21, 872-883. doi:10.1016/j.tplants.2016.07.004

Chen, X.-Y., Liu, L., Lee, E. K., Han, X., Rim, Y., Chu, H., Kim, S.-W., Sack, F. and Kim, J.-Y. (2009). The arabidopsis callose synthase gene gsl8 is required for cytokinesis and cell patterning. *Plant Physiol.* 150, 105-113. doi:10.1104/pp.108.133918

Chen, X.Y. and Kim, J.Y. (2009). Callose synthesis in higher plants. *Plant Signal. Behav.* 4, 489-492. doi:10.4161/psb.4.6.8359

Cortés, J. C. G., Ramos, M., Osumi, M., Pérez, P. and Ribas, J. C. (2016). Fission yeast septation. *Commun. Integr. Biol.* 9, e1189045. doi:10.1080/19420889.2016.1189045

Daher, F. B. and Braybrook, S. A. (2015). How to let go: pectin and plant cell adhesion. *Front. Plant Sci.* 6, 523. doi:10.3389/fpls.2015.00523

de Vries, J. and Archibald, J. M. (2018). Plant evolution: landmarks on the path to terrestrial life. *New Phytol.* 217, 1428-1434. doi:10.1111/nph.14975

Delwiche, C. F. and Cooper, E. D. (2015). The evolutionary origin of a terrestrial flora. *Curr. Biol.* 25, R899-R910. doi:10.1016/j.cub.2015.08.029

Díaz-Cacho, P., Moral, R., Encina, A., Acebes, J. L. and Alvarez, J. (1999). Cell wall modifications in bean (Phaseolus vulgaris) callus cultures tolerant to isoxaben. *Physiol. Plant.* 107, 54-59. doi:10.1034/j.1399-3054.1999.100108.x

Domozych, D. S. (2014). Penium margaritaceum: a unicellular model organism for studying plant cell wall architecture and dynamics. *Plants* 3, 543-558. doi:10.3390/plants3040543

Domozych, D. S., Serfis, A., Kiemle, S. N. and Gretz, M. R. (2007). The structure and biochemistry of charophycean cell walls: I. Pectins of Penium margaritaceum. *Protoplasma* 230, 99-115. doi:10.1007/s00709-006-0197-8

Domozych, D. S., Brechka, H., Britton, A. and Toso, M. (2011). Cell wall growth and modulation dynamics in a model unicellular green alga— penium margaritaceum: live cell labeling with monoclonal antibodies. *J. Bot.* 2011, 1-8. doi:10.1155/2011/632165

Domozych, D. S., Sørensen, I., Popper, Z. A., Ochs, J., Andreas, A., Fangel, J. U., Pielach, A., Sacks, C., Brechka, H., Ruisi-Besares, P. et al. (2014). Pectin metabolism and assembly in the cell wall of the charophyte green alga Penium margaritaceum. *Plant Physiol.* 165, 105-118. doi:10.1104/pp.114.236257

Dong, X. (2004). Functional investigation of *Arabidopsis* callose synthases and the signal transduction pathway. *PhD thesis*, The Ohio State University, Columbus, Ohio.

Drábková, L. Z. and Honys, D. (2017). Evolutionary history of callose synthases in terrestrial plants with emphasis on proteins involved in male gametophyte development. *PLoS ONE* 12, e0187331. doi:10.1371/journal.pone.0187331

Drakakaki, G. (2015). Polysaccharide deposition during cytokinesis: challenges and future perspectives. *Plant Sci.* 236, 177-184. doi:10.1016/j.plantsci.2015.03.018

Drakakaki, G., Robert, S., Szatmari, A.-M., Brown, M. Q., Nagawa, S., Van Damme, D., Leonard, M., Yang, Z., Girke, T., Schmid, S. L. et al. (2011). Clusters of bioactive compounds target dynamic endomembrane networks in vivo. *Proc. Natl. Acad. Sci. USA* 108, 17850-17855. doi:10.1073/pnas.1108581108

Evans, N., Hoyne, P. and Stone, B. (1984). Characteristics and specificity of the interaction of a fluorochrome from aniline blue (sirofluor) with polysaccharides. *Carbohydr. Polym.* 4, 215-230. doi:10.1016/0144-8617(84)90012-2

Fowke, L. C. and Pickett-Heaps, J. D. (1969). Cell division in spirogyra. ii. cytokinesis. *J. Phycol.* 5, 273-281. doi:10.1111/j.1529-8817.1969.tb02614.x

Fraschini, R. (2020). Cytokinesis in eukaryotic cells: the furrow complexity at a glance. *Cells* 9, 271. doi:10.3390/cells9020271

Guseman, J. M., Lee, J. S., Bogenschutz, N. L., Peterson, K. M., Virata, R. E., Xie, B., Kanaoka, M. M., Hong, Z. and Torii, K. U. (2010). Dysregulation of cell-to-cell connectivity and stomatal patterning by loss-of-function mutation in Arabidopsis chorus (glucan synthase-like 8). *Development* 137, 1731-1741. doi:10.1242/dev.049197

Hall, J. D., McCourt, R. M. and Delwiche, C. F. (2008). Patterns of cell division in the filamentous Desmidiaceae, close green algal relatives of land plants. *Am. J. Bot.* 95, 643-654. doi:10.3732/ajb.2007210

Herburger, K. and Holzinger, A. (2015). Localization and quantification of callose in the streptophyte green algae zygnema and klebsormidium: correlation with desiccation tolerance. *Plant Cell Physiol.* 56, 2259-2270. doi:10.1093/pcp/pcv139

Holzinger, A., Herburger, K., Kaplan, F. and Lewis, L. A. (2015). Desiccation tolerance in the chlorophyte green alga Ulva compressa: does cell wall architecture contribute to ecological success? *Planta* 242, 477-492. doi:10.1007/s00425-015-2292-6

Jacobs, A. K., Lipka, V., Burton, R. A., Panstruga, R., Strizhov, N., Schulze-Lefert, P. and Fincher, G. B. (2003). An arabidopsis callose synthase, GSL5, is required for wound and papillary callose formation. *Plant Cell* 15, 2503-2513. doi:10.1105/tpc.016097

Jawaid, M. Z., Sinclair, R., Cox, D. and Drakakaki, G. (2020). A biophysical model for plant cell plate development. *bioRxiv* 2020.05.21.109512. doi:10.1101/2020.05.21.109512

Jiao, C., Sørensen, I., Sun, X., Sun, H., Behar, H., Alseekh, S., Philippe, G., Palacio Lopez, K., Sun, L., Reed, R. et al. (2020). The Penium margaritaceum genome: hallmarks of the origins of land plants. *Cell* 181, 1097-1111.e12. doi:10.1016/j.cell.2020.04.019

Kumar, S., Stecher, G., Li, M., Knyaz, C. and Tamura, K. (2018). MEGA X: molecular evolutionary genetics analysis across computing platforms | molecular biology and evolution | oxford academic. *Mol. Biol. Evol.* 35, 1547-1549. doi:10.1093/molbev/msy096

Lu, S., Wang, J., Chitsaz, F., Derbyshire, M. K., Geer, R. C., Gonzales, N. R., Gwadz, M., Hurwitz, D. I., Marchler, G. H., Song, J. S. et al. (2019). CDD/

SPARCLE: the conserved domain database in 2020. *Nucleic Acids Res.* **48**, D265-D268. doi:10.1093/nar/gkz991

Manfield, I. W., Orfila, C., McCartney, L., Harholt, J., Bernal, A. J., Scheller, H. V., Gilmartin, P. M., Mikkelsen, J. D., Knox, J. P. and Willats, W. G. T. (2004). Novel cell wall architecture of isoxaben-habituated Arabidopsis suspension-cultured cells: global transcript profiling and cellular analysis. *Plant J.* **40**, 260-275. doi:10.1111/j.1365-313X.2004.02208.x

McBride, G. E. (1967). *Cytokinesis in the Green Alga Fritschiella*. Academic Press.

McIntosh, K., Pickett-Heaps, J. D. and Gunning, B. E. (1995). Cytokinesis in Spirogyra: integration of cleavage and cell-plate formation. *Int. J. Plant Sci.* **156**, 1-8. doi:10.1086/297222

Meikle, P. J., Bonig, I., Hoogenraad, N. J., Clarke, A. E. and Stone, B. A. (1991). The location of (1→3)-β-glucans in the walls of pollen tubes of Nicotiana alata using a (1→3)-β-glucan-specific monoclonal antibody. *Planta* **185**, 1-8. doi:10.1007/BF00194507

Miyagishima, S.-Y., Kuwayama, H., Urushihara, H. and Nakanishi, H. (2008). Evolutionary linkage between eukaryotic cytokinesis and chloroplast division by dynamin proteins. *Proc. Natl. Acad. Sci. USA* **105**, 15202-15207. doi:10.1073/pnas.0802412105

Nichols, H. (1973). Handbook of Phycological Methods: Culture Methods and Growth Measurements: Growth Media-Freshwater.

Notredame, C., Higgins, D. G. and Heringa, J. (2000). T-coffee: a novel method for fast and accurate multiple sequence alignment. *J. Mol. Biol.* **302**, 205-217. doi:10.1006/jmbi.2000.4042

Ochs, J., Rue, T. La, Tinaz, B., Yongue, C. and Domozych, D. S. (2014). The cortical cytoskeletal network and cell-wall dynamics in the unicellular charophycean green alga Penium margaritaceum. *Ann. Bot.* **114**, 1237-1249. doi:10.1093/aob/mcu013

Park, E., Díaz-Moreno, S. M., Davis, D. J., Wilkop, T. E., Bulone, V. and Drakakaki, G. (2014). Endosidin 7 specifically arrests late cytokinesis and inhibits callose biosynthesis revealing distinct trafficking events during cell plate maturation. *Plant Physiol.* **165**, 1-16. doi:10.1104/pp.114.241497

Parre, E. and Geitmann, A. (2005). More than a leak sealant. The mechanical properties of callose in pollen tubes. *Plant Physiol.* **137**, 274-286. doi:10.1104/pp.104.050773

Pickett-Heaps, J. D., Gunning, B. E. S., Brown, R. C., Lemmon, B. E. and Cleary, A. L. (1999). The cytoplast concept in dividing plant cells: cytoplasmic domains and the evolution of spatially organized cell division. *Am. J. Bot.* **86**, 153-172. doi:10.2307/2656933

Piršelová, B. and Matušíková, I. (2013). Callose: the plant cell wall polysaccharide with multiple biological functions. *Acta Physiol. Plant.* **35**, 635-644. doi:10.1007/s11738-012-1103-y

Pollard, T. D. (2017). Nine unanswered questions about cytokinesis. *J. Cell Biol.* **216**, 3007-3016. doi:10.1083/jcb.201612068

Popper, Z. A. and Tuohy, M. G. (2010). Beyond the green: Understanding the evolutionary puzzle of plant and algal cell walls. *Plant Physiol.* **153**, 373-383. doi:10.1104/pp.110.158055

Rydahl, M. G., Fangel, J. U., Mikkelsen, M. D., Elisabeth Johansen, I., Andreas, A., Harholt, J., Ulvskov, P., Jørgensen, B., Domozych, D. S. and Willats, W. G. T. (2014). Penium margaritaceum as a model organism for cell wall analysis of expanding plant cells. In *Plant Cell Expansion: Methods and Protocols* (ed. José M. Estevez), pp. 1-21. Springer New York.

Sabba, R. P., Durso, N. A. and Vaughn, K. C. (1999). Structural and immunocytochemical characterization of the walls of dichlobenil-habituated by-2 tobacco cells. *Int. J. Plant Sci.* **160**, 275-290. doi:10.1086/314135

Samuels, A. L., Giddings, T. H. and Staehelin, L. A. (1995). Cytokinesis in tobacco BY-2 and root tip cells: a new model of cell plate formation in higher plants. *J. Cell Biol.* **130**, 1345-1357. doi:10.1083/jcb.130.6.1345

Sawitzky, H. and Grolig, F. (1995). Phragmoplast of the green alga Spirogyra is functionally distinct from the higher plant phragmoplast. *J. Cell Biol.* **130**, 1359-1371. doi:10.1083/jcb.130.6.1359

Scherp, P., Grotha, R. and Kutschera, U. (2001). Occurrence and phylogenetic significance of cytokinesis-related callose in green algae, bryophytes, ferns and seed plants. *Plant Cell Rep.* **20**, 143-149. doi:10.1007/s002990000301

Schindelin, J., Arganda-Carreras, I., Frise, E., Kaynig, V., Longair, M., Pietzsch, T., Preibisch, S., Rueden, C., Saalfeld, S., Schmid, B. et al. (2012). Fiji: An open-source platform for biological-image analysis. *Nat. Methods* **9**, 676-682. doi:10.1038/nmeth.2019

Seguí-Simarro, J. M., Austin, J. R., White, E. A. and Staehelin, L. A. (2004). Electron tomographic analysis of somatic cell plate formation in meristematic cells of arabidopsis preserved by high-pressure freezing. *Plant Cell Online* **16**, 836-856. doi:10.1105/tpc.017749

Shedletzky, E., Shmuel, M., Delmer, D. P. and Lamport, D. T. (1990). Adaptation and growth of tomato cells on the herbicide 2,6-dichlorobenzonitrile leads to production of unique cell walls virtually lacking a cellulose-xyloglucan network1. *Plant Physiol.* **94**, 980-987. doi:10.1104/pp.94.3.980

Smertenko, A., Assaad, F., Baluška, F., Bezanilla, M., Buschmann, H., Drakakaki, G., Hauser, M.-T., Janson, M., Mineyuki, Y., Moore, I. et al. (2017). Plant cytokinesis: terminology for structures and processes. *Trends Cell Biol.* **27**, 885-894. doi:10.1016/j.tcb.2017.08.008

Sørensen, I., Domozych, D. and Willats, W. G. T. (2010). How have plant cell walls evolved? *Plant Physiol.* **153**, 366-372. doi:10.1104/pp.110.154427

Sørensen, I., Pettolino, F. A., Bacic, A., Ralph, J., Lu, F., O'Neill, M. A., Fei, Z., Rose, J. K. C., Domozych, D. S. and Willats, W. G. T. (2011). The charophycean green algae provide insights into the early origins of plant cell walls. *Plant J.* **68**, 201-211. doi:10.1111/j.1365-313X.2011.04686.x

Sørensen, I., Fei, Z., Andreas, A., Willats, W. G. T., Domozych, D. S. and Rose, J. K. C. (2014). Stable transformation and reverse genetic analysis of Penium margaritaceum: a platform for studies of charophyte green algae, the immediate ancestors of land plants. *Plant J.* **77**, 339-351. doi:10.1111/tpj.12375

Starr, R. C. and Zeikus, J. A. (1993). Utex-the culture collection of algae at the university of Texas at austin 1993 list of cultures1. *J. Phycol.* **29**, 1-106. doi:10.1111/j.0022-3646.1993.00001.x

Stewart, K. D., Mattox, K. R. and Floyd, G. L. (1973). Mitosis, cytokinesis, the distribution of plasmodesmata, and other cytological characteristics in the ulotrichales, ulvales, and chaetophorales: phylogenetic and taxonomic considerations. *J. Phycol.* **9**, 128-141. doi:10.1111/j.1529-8817.1973.tb04068.x

Stone, B. and Clarke, A. (1992). Chemistry and Biology of 1, 3-β-Glucans. Carlton, Australia: La Trobe University Press.

Thiele, K., Wanner, G., Kindzierski, V., Jürgens, G., Mayer, U., Pachl, F. and Assaad, F. F. (2009). The timely deposition of callose is essential for cytokinesis in Arabidopsis. *Plant J.* **58**, 13-26. doi:10.1111/j.1365-313X.2008.03760.x

Ulvskov, P., Paiva, D. S., Domozych, D. and Harholt, J. (2013). Classification, naming and evolutionary history of glycosyltransferases from sequenced green and red algal genomes. *PLoS ONE* **8**, e76511. doi:10.1371/journal.pone.0076511

Verma, D. P. S. and Hong, Z. (2001). Plant callose synthase complexes. *Plant Mol. Biol.* **47**, 693-701. doi:10.1023/A:1013679111111

Worden, N., Esteve, V. E., Domozych, D. S. and Drakakaki, G. (2015). Using chemical genomics to study cell wall formation and cell growth in Arabidopsis thaliana and Penium margaritaceum. *Methods Mol. Biol.* **1242**, 23-39. doi:10.1007/978-1-4939-1902-4_2

Wasteneys, G. O., Willingale-Theune, J. and Menzel, D. (1997). Freeze shattering: a simple and effective method for permeabilizing higher plant cell walls. *J. Microsc.* **188**, 51-61. doi:10.1046/j.1365-2818.1977.2390796.x
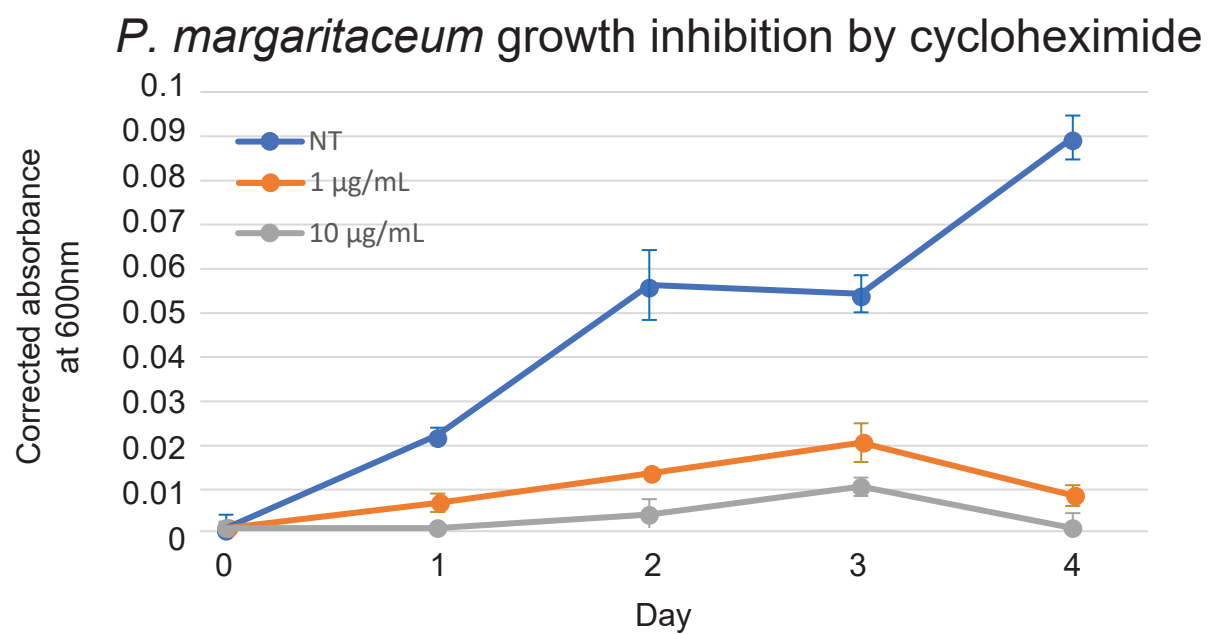
Supplemental Figure 1

Figure S1: *P. margaritaceum* growth inhibition by cycloheximide.

Cycloheximide inhibition of *P. margaritaceum* liquid culture growth over a 4 day

period measured by optical density (OD) at 600 nm. Plot points represent the mean of 3

technical replicates, with s.e.m. shown by the vertical lines.
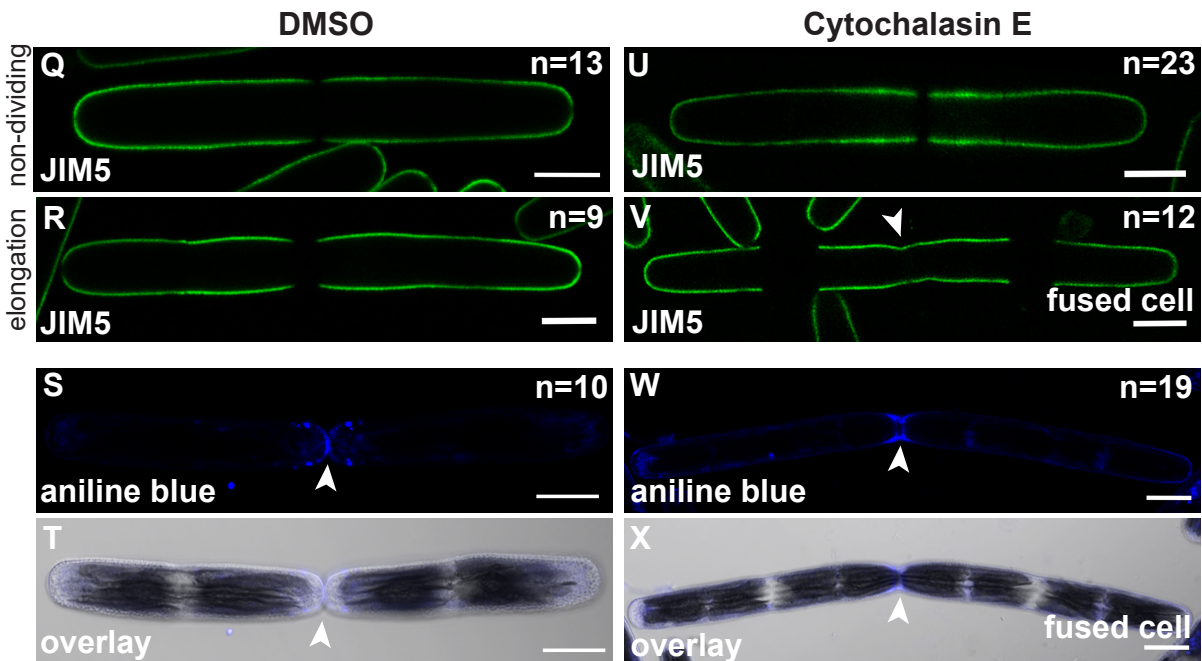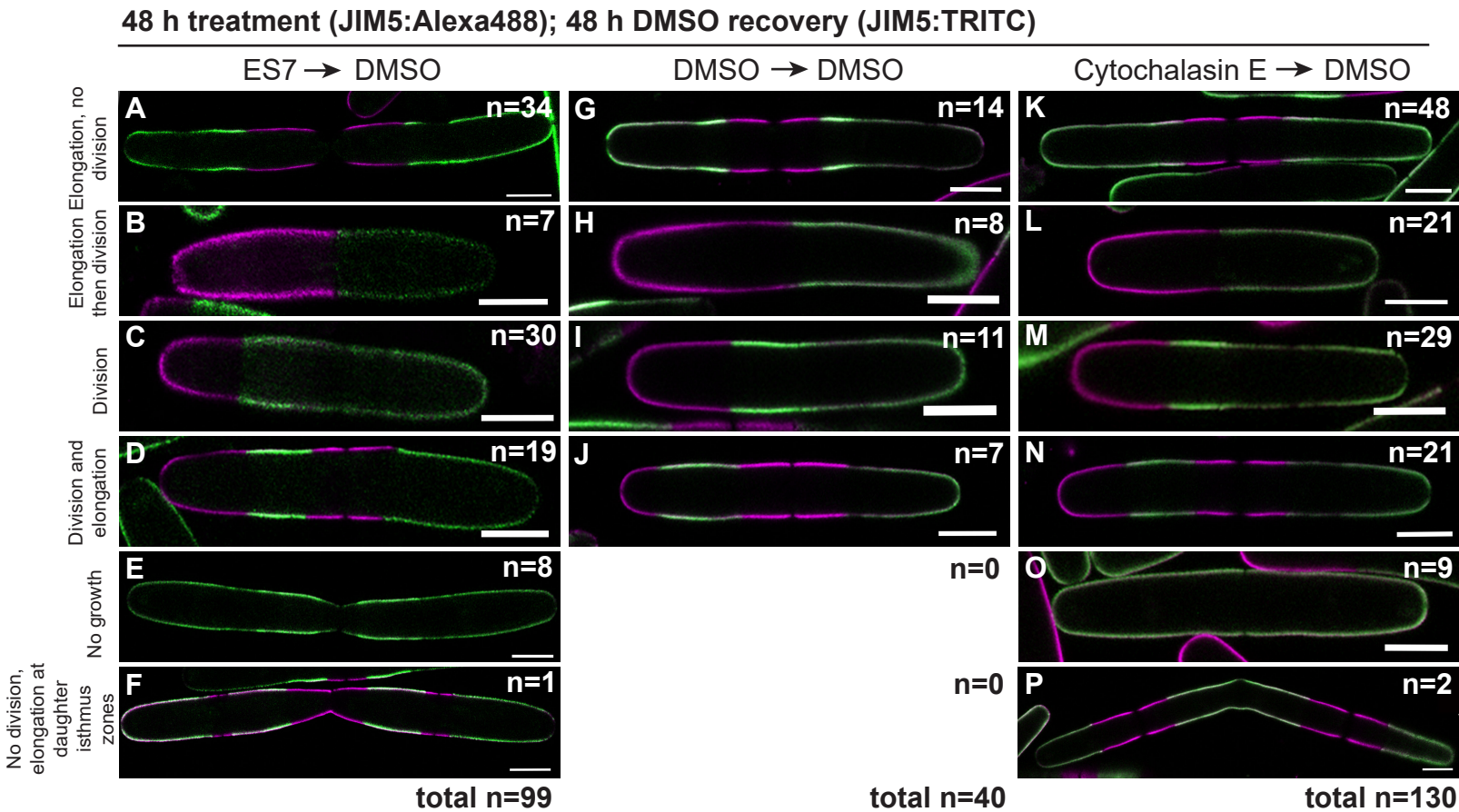
Supplemental Figure 2

Figure S2: Cell wall growth and cell division recovers from ES7 in a majority of cells, revealing a callose-dependent cytokinesis checkpoint.

(A-F) ES7 [50] treated cells were first labeled with JIM5:Alexa488 (green = initial cell wall) then allowed to recover prior to relabeling with JIM5:TRITC (magenta = new growth). Several JIM5 labeled HG patterns were apparent including those indicative of elongation and recently divided cells: (A) an elongating cell with new cell wall growth from the isthmus zone (magenta) prior to division; (B and C) exhibit cells that have recently divided with different levels of prior elongation; (D) recently divided cell (magenta tip) with isthmus zone elongation (central magenta signal). JIM5 relabeling revealed a population of cells (9.1%) that were unable to fully recover from ES7 treatment and 8.5% in the case of cytochalasin E treatment, with some cells exhibiting no new growth (E and O) and others capable of elongation prior to division and elongation at daughter isthmus zones (F and P). DMSO control treated cells (G-J) exhibit common labeling phenotypes with both ES7 and cytochalasin E treated cells, but do not exhibit evidence of cytokinesis defects such as no growth (E and O) and elongation at daughter cell isthmus zones without parental cell cytokinesis (F and P). (Q-X) Representative images of DMSO control treated cells and cytochalasin E treated cells labeled with JIM5:Alexa488 (Q, R, U, V) and aniline blue fluorochrome (S, T, W, X). Mimicking the ES7 effect (Fig. 5), JIM5-labeled cells treated with cytochalasin E show no difference in labeling in non-dividing cells (Q and U), but exhibits JIM5 labeling in the isthmus zone during cell elongation (V, arrowhead). Cytochalasin E does not impact callose deposition at the isthmus zone (W and X, arrowheads). Scale bars = 20 µm.
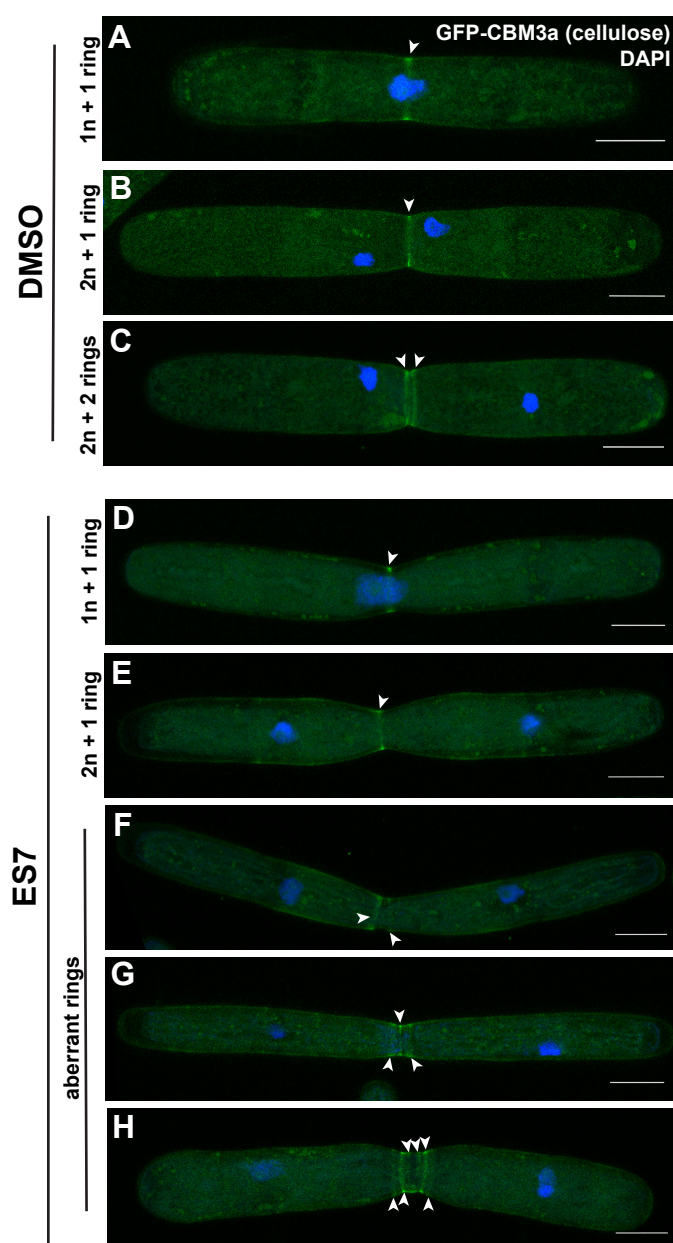
Supplemental Figure 3

Figure S3: Cellulose patterning during cytokinesis under callose inhibition.

(A-C) In DMSO control cells cellulose labeling by GFP-CBM3a was observed in a single isthmus zone ring (A, arrowhead) and diffuse labeling over the entire cell that persisted throughout mitosis (B; n = 8). At the stage where daughter nuclei (blue) migrated to daughter isthmus zones, two cellulose rings were seen at the parental isthmus zone (C, arrowheads; n = 6). (D-H) In ES7-treated cells, normal cellulose ring patterning was observed in interphase (D, arrowhead; n = 2) and immediately following daughter nuclei migration (E, arrowhead; n = 6). In addition, ES7-treated cells exhibited ectopic cellulose rings (n = 3) that varied from multiple (G and H, arrowheads) to improperly localized rings (F, arrowheads). Scale bars = 20 μm. Images are max intensity projections.

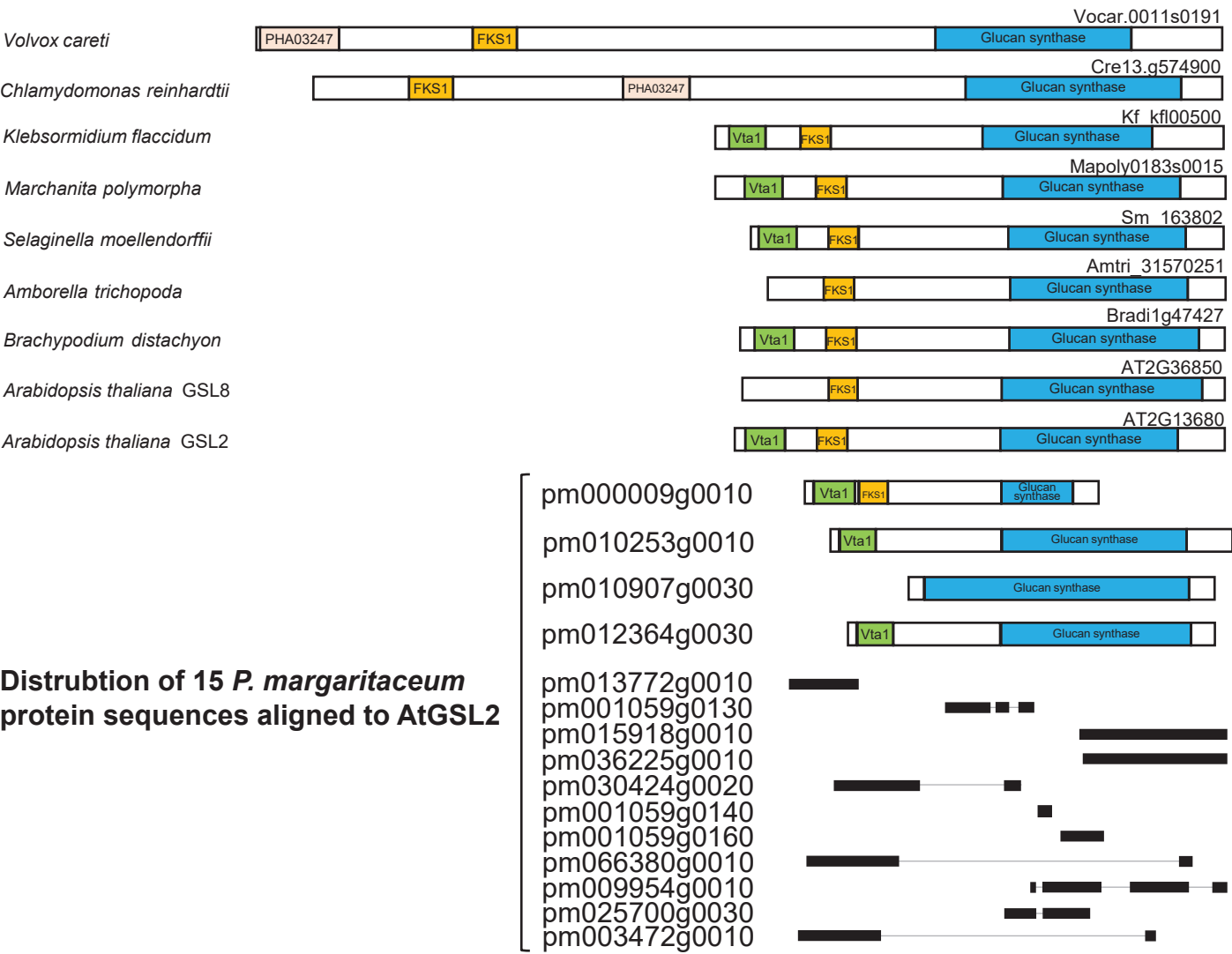## Supplemental Figure 4

Figure S4: Domain analysis of glucan synthase-like enzymes.

Domains recognized by NCBI Conserved Domain Analysis (Shennan Lu et al, 2020) is indicated

by colored boxes and unknown regions are indicated by white boxes. The length of the boxes is

proportional to number of amino acid residues. 15 putative full-length *P. margaritaceum*

protein sequences aligned to AtGSL2 is indicated below AtGSL2, with sequences over 50%

amino acid similarity to AtGSL2 drawn with boxes. The black bars indicate the length of amino

acid similarity coverage and grey lines indicate no similarity of the corresponding region.

Movie 1: Time lapse movie of cytokinesis in *P. margaritaceum*.